

# 1 Macroalgal metabolism and lateral carbon flows can create extended 2 atmospheric CO<sub>2</sub> sinks

3 Kenta Watanabe<sup>1</sup>, Goro Yoshida<sup>2</sup>, Masakazu Hori<sup>2</sup>, Yu Umezawa<sup>3</sup>, Hirotada Moki<sup>1</sup>, and Tomohiro  
4 Kuwae<sup>1</sup>

5 <sup>1</sup>Coastal and Estuarine Environment Research Group, Port and Airport Research Institute, 3-1-1 Nagase, Yokosuka 239-  
6 0826, Japan

7 <sup>2</sup>National Research Institute of Fisheries and Environment of Inland Sea, Japan Fisheries Research and Education Agency, 2-  
8 17-5 Maruishi, Hatsukaichi 739-0452, Japan

9 <sup>3</sup>Department of Environmental Science on Biosphere, Tokyo University of Agriculture and Technology, 3-5-8 Saiwai-cho,  
10 Fuchu, Tokyo 183-8509, Japan

11 *Correspondence to:* Kenta Watanabe (watanabe-ke@p.mpat.go.jp)

12 **Abstract.** Macroalgal beds have drawn attention as one of the vegetated coastal ecosystems that act as atmospheric CO<sub>2</sub>  
13 sinks. Although macroalgal metabolism as well as inorganic and organic carbon flows are important pathways for CO<sub>2</sub>  
14 sequestration by macroalgal beds, the relationships between macroalgal metabolism and associated carbon flows are still  
15 poorly understood. In the present study, we investigated carbon flows, including air–water CO<sub>2</sub> exchange and budgets of  
16 dissolved inorganic carbon, total alkalinity, and dissolved organic carbon (DOC), in a temperate macroalgal bed during  
17 productive months of the year. To assess the key mechanisms responsible for atmospheric CO<sub>2</sub> uptake by the macroalgal bed,  
18 we estimated macroalgal metabolism and lateral carbon flows by using field measurements of carbon species, a field-bag  
19 method, a degradation experiment, and mass-balance modelling in a temperate *Sargassum* bed over a diurnal cycle. Our  
20 results showed that macroalgal metabolism and lateral carbon flows driven by water exchange affected air–water CO<sub>2</sub>  
21 exchange in the macroalgal bed and the surrounding waters. Macroalgal metabolism caused overlying waters to contain low  
22 concentrations of CO<sub>2</sub> and high concentrations of DOC that were efficiently exported offshore from the macroalgal bed.  
23 These results indicate that the exported water can potentially lower CO<sub>2</sub> concentrations in the offshore surface water and  
24 enhance atmospheric CO<sub>2</sub> uptake. Furthermore, the *Sargassum* bed exported 6–33% of the macroalgal net community  
25 production (NCP; 314–1390 mmol-C m<sup>-2</sup> d<sup>-1</sup>) as DOC to the offshore. The results of degradation experiments showed that  
26 56–78% of macroalgal DOC was refractory DOC (RDOC) that persisted for 150 days; thus, the *Sargassum* bed exported 5–  
27 19% of the macroalgal NCP as RDOC. Our findings suggest that macroalgal beds in habitats associated with high water  
28 exchange rates can create extensive CO<sub>2</sub> sinks around them and export a substantial amount of DOC to offshore areas.

## 29 1 Introduction

30 Vegetated coastal ecosystems provide a variety of ecosystem functions that support diverse biological communities and  
31 biogeochemical processes. Recent recognition of the carbon sequestration function of these ecosystems has led to the

32 development of Blue Carbon strategies for mitigating the adverse effects of global climate change via conservation and  
33 restoration of these ecosystems (Nellemann et al., 2009; Duarte et al., 2013; Macreadie et al., 2019).

34 Carbon flows that sequester atmospheric CO<sub>2</sub> in marine ecosystems over timescales of at least several decades are crucial  
35 for the mitigation of climate change (McLeod et al., 2011; Macreadie et al., 2019). Organic carbon burial in sediments is one  
36 of the most important pathways to sequester carbon for a long time (Nellemann et al., 2009; Miyajima et al., 2019).  
37 Evaluation of the carbon sequestration function of vegetated coastal ecosystems has **thus far** been focused on saltmarshes,  
38 seagrasses, and mangroves, which develop their own organic-rich sediments (Macreadie et al., 2019). In contrast, beds of  
39 macroalgae have been assumed to have limited capacity to sequester carbon because they generally settle on hard strata such  
40 as rocks and artificial structures (Krause-Jensen et al., 2018). **Organic matter produced by macroalgae shows variable lability**  
41 **but it is generally more labile than that produced by vascular plants** (Trevathan-Tackett et al., 2015) and hence is **more**  
42 efficiently utilized by consumers and decomposers (Duarte, 1995). However, macroalgal beds are estimated to be the most  
43 extensive vegetated coastal habitats (3.5 million km<sup>2</sup>) in the global ocean, and their global net primary production (1521 Tg-  
44 C yr<sup>-1</sup>) is **larger than** that of other vegetated coastal habitats (Krause-Jensen and Duarte, 2016; Duarte, 2017; Raven, 2018).  
45 **Macroalgal beds therefore have the potential to regulate carbon dynamics in coastal ecosystems.**

46 Other processes in addition to organic carbon burial in on-site sediments must exist for macroalgae to contribute to  
47 atmospheric CO<sub>2</sub> sequestration. Recent studies have proposed that a large fraction of macroalgal production is exported to  
48 other vegetated coastal ecosystems, shelves, and the deep sea, where organic carbon derived from macroalgae can be stored  
49 **in sediments and the water column** for a long time (Krause-Jensen and Duarte, 2016; Krause-Jensen et al., 2018; **Queirós et**  
50 **al., 2019**).

51 **The export and persistence of macroalgal dissolved organic carbon (DOC) has been proposed to be principal processes of**  
52 **macroalgal carbon sequestration, but more empirical support is needed to quantify this carbon flow.** Macroalgal beds export  
53 about 43 % of their production as DOC and particulate organic carbon (POC) (Krause-Jensen and Duarte, 2016). A first-  
54 order estimate has suggested that 33 % of the flux of DOC derived from macroalgae is exported below the mixed layer,  
55 where it contributes to carbon sequestration (Bauer and Druffel, 1998; Krause-Jensen and Duarte, 2016). **Because the**  
56 **proportion of exported carbon that persists for a long time is estimated to be higher in DOC (33%) than in POC (15 %)**  
57 (Krause-Jensen and Duarte, 2016), DOC production, export, and degradation are believed to be significant processes for  
58 carbon sequestration. Although the production of refractory DOC by macroalgae is one of the important factors that impact  
59 carbon sequestration, there are few relevant data (e.g., Wada et al., 2008; Wada and Hama, 2013). The long residence time of  
60 refractory DOC in the water column increases the probability that it reaches depths below the mixed layer.

61 **Even though macroalgal beds perform a significant function by assimilating organic carbon, the chemical kinetics of the**  
62 **carbonate system in the water column could cause them to be net CO<sub>2</sub> emitters via air–water CO<sub>2</sub> exchange.** The dissolved  
63 constituents of the carbonate system must **therefore** be assessed to quantify the effect of community metabolism on air–water  
64 CO<sub>2</sub> exchange (Macreadie et al., 2019; Tokoro et al., 2019). The high rates of macroalgal photosynthesis and respiration  
65 change dissolved inorganic carbon (DIC) concentrations. Calcification and dissolution of associated organisms modify the

66 total alkalinity (TAlk) and DIC. Physical parameters and the balance of the carbonate system decide the magnitude of the  
67 air–water CO<sub>2</sub> exchange (Tokoro et al., 2019). Indeed, some previous studies have shown that macroalgal beds act as sinks  
68 for atmospheric CO<sub>2</sub> (Delille et al., 2009; Ikawa and Oechel, 2015; Koweek et al., 2017) and contribute substantially to  
69 global carbon fluxes (Smith, 1981; Krause-Jensen and Duarte, 2016). Macroalgal metabolism regulates diurnal and temporal  
70 variations in carbonate chemistry and affects calcification by calcifiers in macroalgal beds (Middelboe and Hansen, 2007;  
71 Krause-Jensen et al., 2015, 2016; Duarte and Krause-Jensen, 2018; Wahl et al., 2018). However, there is limited field  
72 evidence for how the effects of macroalgal metabolism on the carbonate system extend to adjacent water bodies.

73 Despite the importance of dissolved carbon flows as CO<sub>2</sub> sequestration pathways, little attention has been paid to  
74 assessing the related carbon budgets in macroalgal beds. In this study, we assessed carbon flows, including air–water CO<sub>2</sub>  
75 exchange and changes of DIC, TAlk, and DOC, in a temperate macroalgal bed during productive periods (winter). To  
76 quantify macroalgal metabolism and dissolved carbon flows, we used a field-bag method, a degradation experiment, and  
77 mass balance modelling. In the present study, we focused on *Sargassum* beds because they are one of the dominant  
78 macroalgal habitats in both temperate and tropical regions (e.g., Fulton et al., 2019; Yoshida et al., 2019). Our goals were to  
79 quantify the contribution of macroalgal beds to atmospheric CO<sub>2</sub> uptake and to investigate the responsible mechanisms on a  
80 daily timescale.

## 81 2 Materials and methods

### 82 2.1 Study site and sample collection

83 This study was conducted in the coastal waters of Heigun Island (33°46'1.7"N, 132°15'24.3"E) in the western Seto Inland  
84 Sea of Japan (Fig. 1). The macroalgal bed at the study site is dominated by *Sargassum* algae (Figs. S1 and S2 in the  
85 Supplement). The surface area of the macroalgal bed is 1.44 ha, and the macroalgal habitat is located at depths shallower  
86 than 5 m (mean depth, 2.0 m). There is no significant freshwater input from the island. The study site is characterized by a  
87 relatively high tidal amplitude (<4 m), and it is adjacent to a deep strait (~60 m).

88 Field surveys were conducted in February and March of 2019 in the macroalgal bed and the adjacent water bodies to take  
89 into account the temporal variations of biotic and abiotic conditions. Winter, including the months of February and March, is  
90 the most productive period of *Sargassum* algae around this study site (Yoshida et al., 2001). Surface water samples for  
91 analyses of DIC, TAlk, and DOC were collected from a research vessel three times (10:00, 13:00, and 16:00) during the  
92 daytime (approximately from 7:00 to 17:00) during both surveys at five stations (H1–H5) (Fig. 1). Four stations (H1–H4)  
93 inside the macroalgal bed were chosen at equal intervals between the ends of the bed to assess average conditions. Station  
94 H5 was established at an offshore site. Samples for DIC and TAlk were dispensed into 250-mL Schott Duran bottles and  
95 preserved with mercuric chloride (200 µL per bottle) to prevent DIC changes due to biological activity. Water samples for  
96 DOC analysis were filtered through 0.2-µm polytetrafluoroethylene filters (DISMIC–25HP; Advantec, Durham, NC, USA)  
97 into precombusted (450 °C for 2 h) 50-mL glass vials and frozen at –20 °C until analysis. At each station, the salinity,

98 temperature, and chlorophyll fluorescence of the surface water were recorded with a RINKO-Profiler (ASTD102, JFE  
99 Advantech, Nishinomiya, Japan).

100 Field bag experiments (e.g., Wada et al., 2007; Towle and Pearse, 1973) were conducted to quantify the changes of DIC,  
101 TAlk, and DOC by macroalgae in February and March of 2019. We selected *Sargassum horneri* as the subject species  
102 because sufficient amounts of *S. horneri* were present in a zone suitable for the experiments. The entire thallus of an  
103 individual *S. horneri* was covered with a plastic bag containing ambient seawater collected in the macroalgal bed. The open  
104 end of the bag was tied at the algal stipe by scuba divers. Triplicate transparent and dark bags were set up to measure the  
105 changes of dissolved constituents due to macroalgal metabolism (Fig. S3 in the Supplement). To assess the effect of  
106 phytoplankton, a set of transparent and dark bags were filled with ambient seawater that was collected in the macroalgal bed  
107 but contained no macroalgae. These bags served as control bags. Water samples from the bags were collected just after the  
108 start of the experiment and about 4 h later through a Tygon® tube by using a hand-held vacuum pump. The collected water  
109 samples were preserved with mercuric chloride (vide supra). After the experiments, the volume of seawater and the wet  
110 weight of the macroalgae in each bag were measured. At the beginning and end of the experiments, the salinity, temperature,  
111 and chlorophyll fluorescence of the surface water were recorded with a RINKO-Profiler (ASTD102, JFE Advantech).  
112 Photosynthetic photon flux was measured with a photon flux sensor (DEFI-L, JFE Advantech) during the experiments.

113 The assessment of the biomass and species composition of the macroalgae was conducted in March 2019. Two 120-m  
114 transect lines were set from the shoreline to the edge of the macroalgal bed to document the biomass, coverage, and species  
115 composition of the macroalgae (Fig. 1). To assess the coverage and species composition, 1 m × 1 m quadrats were located at  
116 10-m intervals along each transect. SCUBA divers quantified the apparent vegetation coverage and species composition in  
117 each quadrat. Five quadrats (0.5 m × 0.5 m) were randomly located in the area dominated by *Sargassum* algae along each  
118 transect to quantify the wet weight biomass (g WW) of the macroalgae. SCUBA divers collected all macroalgae in each  
119 quadrat. The wet weight of the *Sargassum* algae and the other macroalgae were then measured immediately.

## 120 2.2 Degradation experiment

121 DOC samples for degradation experiments were obtained after the field bag experiments. Water samples were collected from  
122 each transparent bag of macroalgae and ambient seawater. The samples were filtered through precombusted (450 °C for 2 h)  
123 glass fibre filters (0.7-µm pore size; GF/F, Whatman, Maidstone, Kent, UK) under reduced pressure. We assumed that GF/F  
124 filters would allow the passage of a significant fraction of free-living bacteria into the experimental samples (e.g., Wada et  
125 al., 2008; Bauer and Bianchi, 2011; Kubo et al., 2015).

126 The 40-mL filtrates were transferred into precombusted (450 °C for 2 h) 100-mL glass vials sealed with rubber and  
127 aluminium caps. The 60-mL headspace in each glass bottle contained about 540 µmol oxygen, which was sufficient to  
128 support the aerobic microbial degradation of DOC (~220 µmol) in each bottle if 1 mol of oxygen was consumed by the  
129 mineralization of 1 mol of DOC into CO<sub>2</sub>. The degradation experiments were conducted based on a total of six incubations  
130 (0, 3, 10, 30, 90, and 150 days) per field survey. Triplicate bottles were used for each incubation. The experimental samples

131 were stored at room temperature (22 °C) in total darkness until analysis. In the present study, we used room temperature for  
132 both samples to evaluate the quality of the organic matter. After incubation, the samples were filtered through 0.2- $\mu\text{m}$   
133 polytetrafluoroethylene filters (DISMIC–25HP; Advantec, Durham, NC, USA) into precombusted (450 °C for 2 h) 100-mL  
134 glass vials and frozen at –20 °C until analysis.

135 In this study, the concentration of refractory DOC (RDOC) was defined as the concentration of DOC remaining after 150  
136 days, and the concentration of DOC derived from macroalgae ( $\text{DOC}_M$ ) was equated to the difference between the DOC  
137 concentration in the macroalgae bag and the DOC concentration in the control bag ( $\text{DOC}_C$ ). Degradation rates ( $k$ ) were  
138 calculated by a first-order exponential decay model as follows:

$$139 \text{DOC}_{M(t)} = \text{DOC}_{M(0)} e^{-kt}, \quad (1)$$

140 where  $\text{DOC}_{M(t)}$  is the amount of  $\text{DOC}_M$  remaining at time  $t$  (day), and  $k$  is the degradation rate ( $\text{day}^{-1}$ ).

### 141 2.3 Sample analyses

142 The DIC concentration and TAlk were determined with a batch-sample analyser (ATT-05 and ATT-15; Kimoto Electric,  
143 Osaka, Japan) according to Tokoro et al. (2014). The analytical precision of the system, based on the standard deviation of  
144 multiple reference replicates, was normally within  $\pm 2 \mu\text{mol L}^{-1}$  for DIC and TAlk.

145 DOC concentrations were measured at least in triplicate with a total organic carbon analyser (TOC-L; Shimadzu, Kyoto,  
146 Japan) as non-purgeable organic carbon according to Ogawa et al. (1999). Potassium hydrogen phthalate (Wako Pure  
147 Industries, Osaka, Japan) adjusted to three concentrations (83, 166, and 332  $\mu\text{M}$ ) was used as a standard for the measurement.  
148 The coefficient of variation of the analyses was less than 2 %.

### 149 2.4 Metabolic parameters

150 Net community production (NCP), gross community production (GCP), community respiration (R), community  
151 calcification (CC), and net DOC release (NDR) were determined from the changes in DIC, TAlk, and DOC of the field bag  
152 experiments. These metabolic parameters were determined for both control and macroalgae as follows:

$$153 \text{Control NCP } (\mu\text{mol-C L}^{-1} \text{ h}^{-1}) = -(\Delta\text{DIC}_{\text{TB}} - \Delta\text{TAlk}_{\text{TB}} / 2) / T \quad (2)$$

$$154 \text{Control R } (\mu\text{mol-C L}^{-1} \text{ h}^{-1}) = (\Delta\text{DIC}_{\text{DB}} - \Delta\text{TAlk}_{\text{DB}} / 2) / T \quad (3)$$

$$155 \text{Control GCP } (\mu\text{mol-C L}^{-1} \text{ h}^{-1}) = \text{Control NCP} - \text{Control R} \quad (4)$$

$$156 \text{Control CC } (\mu\text{mol-C L}^{-1} \text{ h}^{-1}) = (\Delta\text{TAlk}_{\text{TB}} / 2 - \Delta\text{TAlk}_{\text{DB}} / 2) / T \quad (5)$$

$$157 \text{Control NDR } (\mu\text{mol-C L}^{-1} \text{ h}^{-1}) = (\Delta\text{DOC}_{\text{TB}} - \Delta\text{DOC}_{\text{DB}}) / T \quad (6)$$

158  $\text{Macroalgal NCP } (\mu\text{mol-C g WW}^{-1} \text{ h}^{-1}) = -(\Delta\text{DIC}_{\text{TB}} - \Delta\text{TAlk}_{\text{TB}} / 2 - \text{Control NCP}) \times V / B / T$  (7)

159  $\text{Macroalgal R } (\mu\text{mol-C g WW}^{-1} \text{ h}^{-1}) = (\Delta\text{DIC}_{\text{DB}} - \Delta\text{TAlk}_{\text{DB}} / 2 - \text{Control R}) \times V / B / T$  (8)

160  $\text{Macroalgal GCP } (\mu\text{mol-C g WW}^{-1} \text{ h}^{-1}) = \text{Macroalgal NCP} - \text{Macroalgal R}$  (9)

161  $\text{Macroalgal CC } (\mu\text{mol-C g WW}^{-1} \text{ h}^{-1}) = (\Delta\text{TAlk}_{\text{TB}} / 2 - \Delta\text{TAlk}_{\text{DB}} / 2) \times V / B / T$  (10)

162  $\text{Macroalgal NDR } (\mu\text{mol-C g WW}^{-1} \text{ h}^{-1}) = (\Delta\text{DOC}_{\text{TB}} - \Delta\text{DOC}_{\text{DB}}) \times V / B / T$  (11)

163  $\Delta\text{DIC}$ ,  $\Delta\text{TAlk}$ , and  $\Delta\text{DOC}$  were calculated as the final concentrations minus the initial concentrations of the field bag  
 164 experiments. The subscripts TB and DB indicate transparent and dark bags, respectively. The variables  $V$ ,  $B$ , and  $T$  are the  
 165 volume of seawater (L), the wet weight of the macroalgae (g WW), and the incubation time (h) in each bag, respectively.  
 166 The metabolic parameters were converted to daily values per area ( $\text{mmol-C m}^{-2} \text{ d}^{-1}$ ) by using the mean macroalgal biomass,  
 167 the mean water depth, and the lengths of the photoperiods. The photoperiod was defined as the time interval between sunrise  
 168 and sunset; photoperiods were obtained from Automated Meteorological Data Acquisition System (AMeDAS) data provided  
 169 by the Japan Meteorological Agency.

## 170 2.5 Air–water CO<sub>2</sub> flux

171 The air–water CO<sub>2</sub> flux (FCO<sub>2</sub>) was determined by using the bulk formula method. The equation for the method is as  
 172 follows:

173  $\text{FCO}_2 = -KS (\text{fCO}_{2\text{water}} - \text{fCO}_{2\text{air}})$ , (12)

174 where fCO<sub>2</sub> is fugacity. The gas transfer velocity ( $K$ ) was determined from empirical relationships between  $K$  and the wind  
 175 speed above the surface of the water (e.g., Wanninkhof, 1992; McGillis et al., 2001).  $S$  is the CO<sub>2</sub> solubility in the water. A  
 176 positive FCO<sub>2</sub> value indicates CO<sub>2</sub> uptake from the air to the water. Here we used the following empirical equation to  
 177 estimate  $K$  (Wanninkhof, 1992):

178  $K = 0.39U_{10}^2 (Sc / 660)^{-0.5}$ , (13)

179 where  $U_{10}$  is the wind speed at a height of 10 m above the water surface. We determined  $U_{10}$  by assuming that there was a  
 180 logarithmic relationship between wind speed, height, and the roughness of the water surface (Kondo, 2000). Wind speed was  
 181 obtained from AMeDAS data provided by the Japan Meteorological Agency and was measured about 10 km away at  
 182 Agenosho (altitude: 6.5 m). The Schmidt number ( $Sc$ ) was determined from the water temperature and salinity of the water  
 183 surface.

184 The solubility ( $S$ ) of  $\text{CO}_2$  is a function of water temperature and salinity (Weiss, 1974).  $f\text{CO}_{2\text{water}}$  and  $f\text{CO}_{2\text{air}}$  are the  
 185 fugacities of  $\text{CO}_2$  in water and air, respectively.  $f\text{CO}_{2\text{water}}$  was estimated by using chemical equilibrium relationships and the  
 186 TALK and DIC of the water samples (Zeebe and Wolf-Gladrow, 2001). The average salinity and water temperature were used  
 187 to calculate  $f\text{CO}_{2\text{water}}$  in each survey. We used the averaged  $f\text{CO}_{2\text{air}}$  (410  $\mu\text{atm}$ ) measured with a  $\text{CO}_2$  analyser (CO2-09;  
 188 Kimoto Electric, Osaka, Japan).

## 189 2.6 Mass balance modelling

190 We simulated the diurnal changes and budgets of the carbonate system and DOC in the macroalgal bed by using mass  
 191 balance models (Fig. 2). The mass balance models of the macroalgal bed simulated a hypothetical average macroalgal bed  
 192 covering an area of 1  $\text{m}^2$ . The average depth of the hypothetical macroalgal bed was the same as that of the macroalgal bed at  
 193 the study site (2.0 m), and the tide was simulated by changing the water height in synchrony with the observed tide. We used  
 194 the average biomass of *Sargassum* algae obtained from the field survey in the mass balance models. This modelling was  
 195 conducted solely for the macroalgal bed, and the observed values of the offshore site (H5) were used as the boundary  
 196 conditions for carbon inflowing into the macroalgal bed.

197 Time course changes in the concentrations of DIC, TALK, and DOC ( $\mu\text{mol L}^{-1}$ ) in the macroalgal bed were calculated at  
 198 hourly time intervals (Fig. 2). The duration of the simulation was 24 h beginning at sunrise of the survey day. Each  
 199 concentration at time step ( $t$ ) was calculated from the concentration at time step ( $t - 1$ ) as follows:

$$200 \text{DIC}_{(t)} = (\text{DIC}_{(t-1)} - \text{GCP} + \text{R} - \text{CC} + \text{FCO}_2) \times (1 - \text{EX}_{(t)}) + \text{DIC}_O \times \text{EX}_{(t)} \quad (14)$$

$$201 \text{TALK}_{(t)} = (\text{TALK}_{(t-1)} - 2\text{CC}) \times (1 - \text{EX}_{(t)}) + \text{TALK}_O \times \text{EX}_{(t)} \quad (15)$$

$$202 \text{DOC}_{(t)} = (\text{DOC}_{(t-1)} + \text{NDR}) \times (1 - \text{EX}_{(t)}) + \text{DOC}_O \times \text{EX}_{(t)} \quad (16)$$

203 Metabolic parameters (GCP, R, CC, and NDR) were determined from the results of the field bag experiments (Fig. 2 and  
 204 Table S1 in the Supplement). These metabolic parameters were calculated as the sum of the contributions from both  
 205 macroalgae and phytoplankton. The parameters  $\text{DIC}_O$ ,  $\text{TALK}_O$ , and  $\text{DOC}_O$  in Eqs. (14–16) are the mean values of DIC, TALK,  
 206 and DOC, respectively, at the offshore station (H5), and the initial values in the simulation were equated to those values.  
 207 Namely,  $\text{DIC}_{(0)}$ ,  $\text{TALK}_{(0)}$ , and  $\text{DOC}_{(0)}$  were equated to  $\text{DIC}_O$ ,  $\text{TALK}_O$ , and  $\text{DOC}_O$ , respectively. We assumed that there was no  
 208 biogeochemical exchange between the bottom substrate and water. In the simulation, we assumed that the metabolic  
 209 parameters (GCP, R, CC, and NDR) of *S. horneri* were applied to the entire macroalgal bed and used different metabolic  
 210 parameters for day and night.  $\text{EX}$  ( $0 \leq \text{EX} \leq 1$ ), the hourly water exchange rate, was defined as follows:

$$211 \text{EX}_{(t)} = \text{EX}_{\text{tide}(t)} + \text{EX}_r, \quad (17)$$



$$212 \quad EX_{tide(t)} = \begin{cases} (H_{(t)} - H_{(t-1)}) / H_{(t)} & (H_{(t)} \geq H_{(t-1)}) \\ 0 & (H_{(t)} < H_{(t-1)}) \end{cases} \quad (18)$$

213  $EX_{tide}$  indicates the water exchange rate due to tidal change.  $EX_{tide}$  was estimated from the changes of water height ( $H$ ) and  
 214 was positive during the flood tide and zero during the ebb tide.  $EX_r$  was defined as the residual exchange rate due to factors  
 215 other than tidal exchange. The value of  $EX_r$  was chosen so as to minimize the root mean square error (RMSE) of the  
 216 modelled values versus the observed values. RMSEs were calculated for the  $z$ -scores of DIC, TALK, DOC, and  $fCO_2$ , which  
 217 were equated to the differences between the modelled values and the means of the observed values divided by the standard  
 218 deviations of the observed values. The value of  $EX_r$  that minimized the averaged RMSEs for these four parameters was  
 219 determined for each survey. This model fitting was performed using the daytime data. The estimated  $EX_r$  was applied  
 220 throughout the diurnal cycle on the assumption that  $EX_r$  was comparable during the day and night. We ran two different  
 221 model scenarios, one with and the other without water exchange.

222 The budgets of DIC, TALK, and DOC were calculated as the net gain or loss of each constituent due to water exchange.  
 223 The changes in  $fCO_2$ , which were estimated by using chemical equilibrium relationships and the TALK and DIC of the water  
 224 samples (Zeebe and Wolf-Gladrow, 2001), were used to calculate  $fCO_2$ . The average salinity and water temperature were  
 225 used to calculate  $fCO_2$  in each survey.

## 226 2.7 Statistical analyses

227 Statistical analyses were performed by using R statistical packages (R Core Team, 2019). We used a Welch's two-sample  $t$ -  
 228 test to determine whether there were differences in salinity, DIC, TALK,  $fCO_2$ , and DOC between the macroalgal bed and the  
 229 offshore site and to detect the differences between the initial and final concentrations of DOC during degradation  
 230 experiments.

## 231 3 Results

### 232 3.1 Carbonate system and DOC in the macroalgal bed

233 There were no differences in salinity and TALK between the macroalgal bed ( $n = 12$ ) and the offshore site ( $n = 3$ ) in either  
 234 February or March (Welch's two-sample  $t$ -test,  $p > 0.05$ ) (Fig. 3 and Table S2 in the Supplement). The DIC concentration  
 235 was significantly lower in the macroalgal bed ( $1964 \pm 22 \mu\text{mol L}^{-1}$ ) than at the offshore site ( $1991 \pm 1 \mu\text{mol L}^{-1}$ ) in February  
 236 ( $p = 0.002$ ) (Fig. 3 and Table S2 in the Supplement). In March, the variation of the DIC concentration was large ( $1962 \pm 43$   
 237  $\mu\text{mol L}^{-1}$ ) in the macroalgal bed but was also significantly lower than at the offshore site ( $1992 \pm 1 \mu\text{mol L}^{-1}$ ) ( $p = 0.033$ ).  
 238 The  $fCO_2$  values were significantly lower in the macroalgal bed than at the offshore site in both February ( $p = 0.001$ ) and  
 239 March ( $p = 0.025$ ) (Fig. 3 and Table S2 in the Supplement). The  $fCO_2$  values in the macroalgal bed (February,  $265 \pm 31$   
 240  $\mu\text{atm}$ ; March,  $272 \pm 49 \mu\text{atm}$ ) and the offshore site (February,  $305 \pm 3 \mu\text{atm}$ ; March,  $309 \pm 1 \mu\text{atm}$ ) were lower than  $fCO_{2\text{air}}$



241 (410  $\mu\text{atm}$ ). The DOC concentration was significantly higher in the macroalgal bed than at the offshore site during March ( $p$   
242 = 0.010), but there was no significant difference between the two during February ( $p > 0.05$ ) (Fig. 3 and Table S2 in the  
243 Supplement).  $f\text{CO}_2$  was strongly correlated with DIC in both February and March (Fig. 4). The homogeneous buffer factors  
244 ( $\beta$ ), which were equated to the slopes of log-log plots of  $f\text{CO}_2$  versus DIC, were 10.81 and 9.36 in February and March,  
245 respectively.

246 Community carbon metabolism was calculated from the field-bag experiments (Table 1 and Table S1 in the Supplement).  
247 The NCP of macroalgae was about four times higher in March (1390  $\text{mmol-C m}^{-2} \text{d}^{-1}$ ) than in February (314  $\text{mmol-C m}^{-2}$   
248  $\text{d}^{-1}$ ) (Table 1) and was considerably higher than that of phytoplankton ( $\sim 13 \text{ mmol-C m}^{-2} \text{d}^{-1}$ ). The net community  
249 calcification (NCC) of macroalgae was positive ( $\sim 21 \text{ mmol-C m}^{-2} \text{d}^{-1}$ ), but the values were much lower than the NCP values.  
250 The net DOC release rates of macroalgae were 107  $\text{mmol-C m}^{-2} \text{d}^{-1}$  and 88  $\text{mmol-C m}^{-2} \text{d}^{-1}$  in February and March,  
251 respectively. These values were equivalent to about 34 % and 6 % of the NCP in February and March, respectively.

### 252 3.2 Biomass and species composition of macroalgae

253 The macroalgal bed was dominated by *Sargassum* algae (Fig. 5 and Figs. S1 and S2 in the Supplement). The biomass of  
254 *Sargassum* algae (mean: 4693  $\text{g WW m}^{-2}$ ) was higher than that of the other macroalgae (264  $\text{g WW m}^{-2}$ ) (Fig. 5). The  
255 coverage of *Sargassum* algae ( $\sim 80$  %) was also larger than that of the other macroalgae ( $\sim 51$  %).

### 256 3.3 Degradation of DOC

257 DOC concentrations collected from macroalgae bags decreased with time in both experiments (Welch's two-sample  $t$ -test,  $p$   
258  $< 0.05$ ; Fig. 6). In contrast, DOC concentrations collected from control bags were stable during the experiments ( $p > 0.05$ ).  
259  $\text{DOC}_M$  gradually decreased with time. Refractory  $\text{DOC}_M$  ( $\text{RDOC}_M$ ) concentrations were  $56 \pm 4$  % and  $78 \pm 27$  % of initial  
260  $\text{DOC}_M$  concentrations in February and March, respectively (Fig. 6c). Degradation rates ( $k$ ) for 150-day incubations were  
261  $0.0044 \text{ d}^{-1}$  and  $0.0021 \text{ d}^{-1}$  in February and March, respectively.

### 262 3.4 Carbon budgets estimated using mass balance models

263 The mass balance models simulated the temporal changes of carbonate chemistry and DOC concentrations for the two model  
264 scenarios, that is, with and without considering water exchange (Fig. 3). The mean RMSEs for the best-fitting model  
265 (February, 0.55; March, 0.86) were lower than those for the model assuming that  $EX$  was zero (February, 3.85; March, 3.13)  
266 (Table 2). The fitted model that took into consideration  $EX$  improved the RMSEs of all parameters in February. In March,  
267 the RMSEs of DIC and  $f\text{CO}_2$  were improved by the model fitting, but those of DOC and TALK changed little (Table 2). The  
268 estimated  $EX_r$  values were 39 % and 43 % in February and March, respectively (Table 3). Hourly water exchange rates (the  
269 sum of  $EX_{\text{tide}}$  and  $EX_r$ ) were estimated to be 39–52 % and 43–69 % in February and March, respectively (Fig. 3 and Table 3).

270 DIC concentrations were decreased in the daytime by primary production (Fig. 3a, f). TALK values in the macroalgal bed  
271 were stable and very similar to the TALK values of the offshore seawater (Fig. 3b, g). The  $f\text{CO}_2$  decreased during the daytime

272 because of the concurrent decrease of the DIC concentration (Fig. 3c, h). DOC concentrations in the macroalgal bed  
273 exceeded those at the offshore site during the daytime (Fig. 3d, i).

274 DIC budgets driven by water exchange indicated a net input of DIC from offshore to the macroalgal bed (Fig. 7 and  
275 Table 3). The areal influxes of DIC were  $337 \text{ mmol-C m}^{-2} \text{ d}^{-1}$  and  $1387 \text{ mmol-C m}^{-2} \text{ d}^{-1}$  in February and March,  
276 respectively. These fluxes were almost equivalent to the sum of NCP, NCC, and  $\text{FCO}_2$  in the macroalgal bed (Fig. 7). DOC  
277 was exported from the macroalgal bed to offshore (Fig. 7). The areal effluxes of DOC (February:  $125 \text{ mmol-C m}^{-2} \text{ d}^{-1}$ ,  
278 March:  $96 \text{ mmol-C m}^{-2} \text{ d}^{-1}$ ) were similar to the NDRs. The export fluxes of  $\text{RDOC}_M$  were estimated to be  $59 \text{ mmol-C m}^{-2}$   
279  $\text{d}^{-1}$  and  $67 \text{ mmol-C m}^{-2} \text{ d}^{-1}$  in February and March, respectively (Fig. 7). The  $\text{FCO}_2$  values showed that both the macroalgal  
280 bed and the offshore site took up atmospheric  $\text{CO}_2$  during these study periods.  $\text{FCO}_2$  values were higher in the macroalgal  
281 bed than offshore during both periods (Fig. 7 and Table 3).

## 282 4 Discussion

### 283 4.1 $\text{CO}_2$ uptake and DIC budgets in the macroalgal bed

284 Atmospheric  $\text{CO}_2$  uptake was affected by community metabolism and water exchange, which regulated the carbon budget in  
285 the *Sargassum* algae-dominated macroalgal bed. Positive NCP values showed that the macroalgal bed acted as an  
286 autotrophic system during the study periods. Macroalgal DIC uptake (i.e., NCP) accounted for >97 % of total NCP in this  
287 system (Table 1); the rest was attributable to planktonic NCP. Biological uptake of DIC promoted atmospheric  $\text{CO}_2$  uptake  
288 by contributing to the decrease of DIC concentrations and  $\text{fCO}_2$  during the day inside the macroalgal bed (Figs. 3 and 7).

289 Previous studies have shown that macroalgal primary production reduces DIC and  $\text{CO}_2$  concentrations. For example,  
290 DIC uptake by kelp reduces  $\text{fCO}_2$  and thereby contributes to the uptake of atmospheric  $\text{CO}_2$  inside kelp beds (Delille et al.,  
291 2000, 2009; Koweek et al., 2017; Pfister et al., 2019). The aquaculture of macroalgal species such as the kelp *Laminaria*  
292 *japonica* and the red alga *Gracilaria lemaneiformis* has also been shown to result in annual net uptake of  $\text{CO}_2$  because of  
293 active photosynthesis by the macroalgae (Jiang et al., 2013). In contrast, knowledge about in situ carbonate chemistry in beds  
294 of *Sargassum* algae is limited (e.g., Tokoro et al., 2019). The present study, however, has shown that a bed of *Sargassum*  
295 algae takes up atmospheric  $\text{CO}_2$  over a diurnal cycle during productive periods of the year.

296 Our results showed that metabolism and water exchange regulated the diurnal variations in DIC and  $\text{fCO}_2$  in the  
297 macroalgal bed. Our mass balance model analyses suggested that the high rate of water inflow from the outside the bed  
298 strongly affected DIC concentrations and  $\text{fCO}_2$  in the macroalgal bed (Fig. 3a, f). The decrease of the DIC concentration of  
299 the macroalgal bed was moderated by water exchange during the day. The high rate of water exchange reduced the  
300 difference in  $\text{FCO}_2$  between the inside and outside of the macroalgal beds (Fig. 7). Conversely, water characterized by low  
301 DIC and  $\text{fCO}_2$  values was efficiently exported from the macroalgal bed to the surrounding water (Fig. 7). Our findings  
302 therefore suggested that macroalgal beds can create areas of adjacent water that serve as  $\text{CO}_2$  sinks. Previous studies have  
303 proposed that a canopy of the kelp genus *Macrocystis* dampens water exchange (Rosman et al., 2007), and the residence time

304 of water within kelp beds can reach several days (Jackson and Winant, 1983; Delille et al., 2009). In contrast, the exposed  
305 side of a kelp bed is very much affected by the advection of offshore water (Koweek et al., 2017). Water exchange rates are  
306 affected by the surface area of beds, canopy development, topography, and hydrological conditions.

307 The seasonality of the growth of macroalgae regulates the seasonal variations of carbonate chemistry and sink/source  
308 behaviour (Delille et al., 2009; Koweek et al., 2017). Annual fluctuations of the surface area of kelp beds affect interannual  
309 variations in air–sea CO<sub>2</sub> fluxes in adjacent water bodies (Ikawa and Oechel, 2015). In the present study, we focused on how  
310 daily carbon budgets were related to macroalgal metabolism and hydrological conditions during productive periods. The  
311 biomass of *Sargassum* algae fluctuates seasonally and increases in winter (from November to April) around the present study  
312 site (Yoshida et al., 2001). Future studies should assess the seasonal variability of carbonate chemistry in *Sargassum* beds.

313 The homogenous buffer factor ( $\beta$ ) is a general and helpful tool that can be used to identify the main processes that affect  
314 carbonate chemistry dynamics (e.g., Frankignoulle, 1994). Frankignoulle (1994) found the relationship  $\beta = -7.02 + 0.186$   
315  $\times \%C_{org}$ , where  $\%C_{org}$  is the percent change of the DIC concentration due to photosynthesis and respiration. By using this  
316 equation, we calculated the  $\%C_{org}$  to be 96 % and 88 % in February and March, respectively (Fig. 4). The results therefore  
317 indicate that NCP was the main regulator of carbonate chemistry, and the contribution of NCC was relatively small. This  
318 conclusion is consistent with the results of the field bag experiments (Table 1).

#### 319 4.2 Community metabolism in the macroalgal bed

320 Macroalgal NCP values in the present study (314–1390 mmol-C m<sup>-2</sup> d<sup>-1</sup>) were comparable to those in a sub-Arctic kelp bed  
321 (~1250 mmol-C m<sup>-2</sup> d<sup>-1</sup>; Delille et al., 2009) and to gross primary production in a *Macrocystis* kelp bed in California (~570  
322 mmol-C m<sup>-2</sup> d<sup>-1</sup>; Towle and Pearse, 1973; Jackson, 1987) and in an *Ecklonia* kelp bed (464 mmol-O<sub>2</sub> m<sup>-2</sup> d<sup>-1</sup>; Randall et al.,  
323 2019); they were much larger than the NCP values in a calcareous macrophyte bed (19 mmol-C m<sup>-2</sup> d<sup>-1</sup>; Bensoussan and  
324 Gattuso, 2007), in temperate maerl beds (-38 mmol-C m<sup>-2</sup> d<sup>-1</sup>; Martin et al., 2007), and on a coral reef dominated by green  
325 and red algae (-112 to 61 mmol-C m<sup>-2</sup> d<sup>-1</sup>; Falter et al., 2001). The suppression of macroalgal R by low water temperatures  
326 during the productive winter can explain the relatively high NCP values observed at our study site (Table 1 and Table S1 in  
327 the Supplement). The macroalgal NCP value during March was four times higher than the value during February in the  
328 present study (Table 1). Irradiance, length of the photoperiod, and growth phase collectively control the temporal variations  
329 of macroalgal NCP. In the present study, both surveys were conducted during the productive period, but the difference in the  
330 averaged biomass per individual *S. horneri* used for the field bag experiments (February, 353 g WW; March 260 g WW)  
331 may indicate a difference in growth phase.

332 The relative growth rates (% d<sup>-1</sup>) of *S. horneri* were calculated to be 1.2–7.4 % d<sup>-1</sup> based on the ratio of growth (= NCP  
333 – NDR) to biomass (Table S1 in the Supplement). To calculate biomass, we assumed that the water content was 85 % of the  
334 wet weight and that carbon content was 30 % of the dry weight (Watanabe et al., unpublished data). These relative growth  
335 rates were comparable to estimates based on biomass changes of *S. horneri* (around 4 % d<sup>-1</sup>, Gao and Hua, 1997; Choi et al.,  
336 2008) and *S. muticum* (~10 % d<sup>-1</sup>, Pedersen et al., 2005).

337 The estimated uncertainties of NCC and NCP derived from the measurement precision of TALK and DIC were ~13  
338  $\text{mmol-C m}^{-2} \text{d}^{-1}$  and ~26  $\text{mmol-C m}^{-2} \text{d}^{-1}$ , respectively. These uncertainties were similar to NCC values (macroalgae, 11–21  
339  $\text{mmol-C m}^{-2} \text{d}^{-1}$ ; phytoplankton, -12–3  $\text{mmol-C m}^{-2} \text{d}^{-1}$ ) and phytoplankton NCP values (9–13  $\text{mmol-C m}^{-2} \text{d}^{-1}$ ) (Table 1).  
340 It is therefore difficult to discuss NCC values and phytoplankton NCP values quantitatively, but these values were  
341 substantially lower than macroalgal NCP values in this study. Increasing the incubation time in the field bag experiments  
342 should help to reduce these uncertainties.

#### 343 4.3 Refractory DOC release by macroalgae

344 Our results showed that the *Sargassum* bed released a large amount of DOC (Fig. 7). Most of the released DOC was  
345 exported out of the macroalgal bed via water exchange during the day. The DOC release rates of *S. horneri* (18.7–22.8  $\mu\text{mol-}$   
346  $\text{C g WW}^{-1} \text{d}^{-1}$ , Table S1 in the Supplement) were within the range of those reported for *Ecklonia* kelp (1.5–72.5  $\mu\text{mol-C g}$   
347  $\text{WW}^{-1} \text{d}^{-1}$ , Wada et al., 2007), which were calculated by assuming that water content was 85 % of wet weight (Watanabe et  
348 al., unpublished data). The fact that Wada et al. (2007) collected data over an entire year, whereas our data were collected  
349 during only the most productive two months of the year, accounts for the difference in the variations of DOC release rates.  
350 Previous studies have found that a substantial portion of production is released as DOC by kelps (18–62 %, Abdullah and  
351 Fredriksen, 2004; Wada et al., 2007). Our results showed that *Sargassum* algae sometimes release a similar percentage of  
352 production as DOC (6–34%). Although the DOC release rates were similar between our two surveys, the percentages were  
353 very different between February (34 %) and March (6 %) (Fig. 7). DOC release rates by kelps have been shown to be  
354 correlated with irradiance, but irradiance explained only 13 % of the variation of the DOC release rates (Reed et al., 2015).  
355 Time lags between light-stimulated carbon assimilation and DOC release may explain some of the variation between  
356 irradiance and DOC release. High-frequency time-series measurements may help to explain the daily variations of  
357 macroalgal carbon metabolism. In this study, the reproducibility of the DOC mass balance model (i.e., the improvement of  
358 RMSEs) differed between the February and March data sets (Fig. 3 and Table 2). Temporal and interspecific variations of  
359 DOC release rates may have caused this difference.

360 Refractory organic carbon acts as a carbon reservoir in seawater (Hansell and Carlson, 2015) and is considered to be one  
361 of the important contributors to carbon sequestration by coastal macrophytes (Maher and Eyre, 2010; Watanabe and Kuwae,  
362 2015; Krause-Jensen and Duarte, 2016; Duarte and Krause-Jensen, 2017). Our results show that the *Sargassum* bed exported  
363 5–19% of the macroalgal NCP as RDOC that persisted for 150 days (Fig. 7). The fact that the degradation rates of  
364 macroalgal DOC are lower than those of DOC released by phytoplankton ( $k$  values,  $> 0.025 \text{d}^{-1}$ ; Hama et al., 2004;  
365 Kirchman et al., 1991) implies that macroalgal DOC is more biologically recalcitrant than DOC produced by phytoplankton  
366 (Wada et al., 2008). Previous studies have suggested that macroalgae produce phenolic compounds such as phlorotannin that  
367 are biologically recalcitrant (Swanson and Druehl, 2002; Wada and Hama, 2013; Powers et al., 2019). A thermogravimetric  
368 approach has also shown that macroalgal thalli contain refractory compounds (Trevathan-Tackett et al., 2015), some of

369 which are released as the plant grows. These findings indicate that macroalgae release chemically recalcitrant DOC for  
370 decomposers.

371 Wada et al. (2008) have estimated the turnover times of the DOC released by *Ecklonia* kelp, the reciprocals of the  
372 degradation rates ( $k$ ), to be 24–172 days (i.e.,  $k$  values of 0.0058–0.0407 d<sup>-1</sup>) during 30-days incubations. In the present  
373 study, the turnover times of DOC released by *S. horneri* were calculated to be 111–238 days (i.e.,  $k$  values for 30-day  
374 incubations of 0.0042–0.0090 d<sup>-1</sup>), longer than the turnover times of *Ecklonia* kelp. These findings indicate that the  
375 recalcitrance of macroalgal DOC is variable and depends on the species and environmental conditions. The phlorotannin  
376 contents of macroalgal thalli vary among seasons, growth phases, and species (Steinberg, 1989; Kamiya et al., 2010), and  
377 these variations may regulate seasonal and interspecific variations in the biological recalcitrance of macroalgal DOC.  
378 Furthermore, degradation rates for 150-day incubations (0.0021–0.0044 d<sup>-1</sup>; Fig. 6) were slower than those for first 30-day  
379 incubations, indicating that relatively short duration degradation experiments may underestimate the long-term persistence of  
380 OC (e.g., Trevathan-Tackett et al., 2020).

381 The microbial degradation of DOC is also affected by temperature, and high temperature stimulates DOC degradation  
382 (e.g., Chen and Wangersky, 1996; Lønborg and Álvarez-Salgado, 2012). In this study, the degradation rates of DOC should  
383 be overestimated compared to in situ conditions because the incubation temperature for the degradation experiments (22 °C)  
384 was higher than the in situ temperature (~13 °C, Table 1). The difference in the initial DOC<sub>M</sub> concentrations in the  
385 macroalgae bags between February and March may have been caused by the differences in the biomass of macroalgae and  
386 volume of water in the experimental bags (Fig. 6a, b). Variations of DOC concentrations may affect degradation rates via  
387 resource limitation of microbial activity (e.g., Arrieta et al., 2015). Understanding of the fate of macroalgal DOC would be  
388 enhanced by the assessment of the physical and biochemical factors that regulate microbial degradation of DOC.

389 Ogawa et al. (2001) have shown that marine bacteria take up labile organic matter (OM) such as glucose and convert it  
390 into refractory OM. Some of the macroalgal DOC may be converted to refractory OC by microbes and persist in water for a  
391 long time. Carbon flows through the microbial loop should be assessed as one of the fates of OM derived from macroalgal  
392 beds.

#### 393 **4.4 Implications for the CO<sub>2</sub> sequestration function of macroalgae**

394 Macroalgal beds are considered as potential carbon-donor sites in the context of Blue Carbon sequestration (Krause-Jensen  
395 et al., 2018). The export of particulate macroalgal carbon (e.g., entire thalli and fragments) to the deep sea via physical  
396 processes would contribute to CO<sub>2</sub> sequestration (Krause-Jensen and Duarte 2016; Filbee-Dexter et al., 2018; Pessarrodona  
397 et al., 2018; Kokubu et al., 2019; Pedersen et al., 2019) (Fig. 2). The export of recalcitrant DOC from macroalgal beds is also  
398 anticipated to be an important pathway of CO<sub>2</sub> sequestration (Wada and Hama, 2013; Barrón et al., 2014; Reed et al., 2015).  
399 A first-order assessment has suggested that almost 70% of global macroalgal carbon sequestration is attributable to DOC  
400 export to the deep sea (Krause-Jensen and Duarte, 2016). Our results showed that a *Sargassum* bed released substantial  
401 amount of RDOC, which was rapidly exported from the habitat to the offshore. The residence time of ~200 days for

402 dissolved matter in the western Seto Inland Sea (Balotro et al., 2002) indicates that macroalgal DOC can be exported to the  
403 outside of the inland sea and can reach the deep sea via vertical mixing.

404 The decrease in  $f\text{CO}_2$  due to macroalgal DIC uptake directly controls the influx of atmospheric  $\text{CO}_2$  into macroalgal  
405 habitats and the waters surrounding them. The present study showed that the metabolism of *Sargassum* algae mediated the  
406 production of low-DIC and low- $f\text{CO}_2$  water, which was rapidly exported to outside the habitat. Because macroalgae  
407 commonly inhabit rocky reefs facing the open ocean, macroalgal metabolism may affect a wide range of water bodies  
408 surrounding rocky reef habitats (e.g., Ikawa and Oechel, 2015). The  $\text{CO}_2$  sequestration function of macroalgae found in  
409 habitats where macroalgae-affected water easily diffuses offshore has been overlooked.

410 Studies of the role of macroalgae in  $\text{CO}_2$  sequestration should use field observations and coupled ecological-physical  
411 models to assess the spatial spread and fate of DOC and low- $f\text{CO}_2$  waters derived from macroalgal habitats (Kuwae et al.,  
412 2019; Macreadie et al., 2019). Because coastal primary producers other than macroalgae can also be a source of low- $f\text{CO}_2$   
413 and high-DOC waters, separately analysing the fate of these waters would help shed light on the role of these ecosystems.  
414 Seasonal variations in oceanographic and climatic conditions regulate the transport of waters affected by macroalgae. Such  
415 studies will lead to a better understanding of the role of macroalgae in sequestering Blue Carbon and thereby mitigating  
416 global climate change.

## 417 **5 Conclusions**

418 The present study showed that macroalgal metabolism and lateral carbon flows regulated carbon budgets and air–water  $\text{CO}_2$   
419 exchange in a temperate macroalgal bed and its surrounding water. Macroalgae took up DIC via photosynthesis and released  
420 large amounts of DOC to the offshore waters adjacent to the bed. Hydrological water exchange enhanced the lateral carbon  
421 flows and the spread of low- $f\text{CO}_2$  and high-DOC water mediated by macroalgal metabolism to the surrounding water. Our  
422 findings suggest that macroalgal beds have the potential to create areas of adjacent water that serve as  $\text{CO}_2$  sinks. These  
423 results suggest the need for future research to assess the areal extent and fate of macroalgae-mediated low- $f\text{CO}_2$  and high-  
424 DOC waters.

## 425 **Data availability**

426 Research data can be accessed by contacting the authors.

## 427 **Author contributions**

428 KW, GY, MH, YU, and TK conceived the study. KW, GY, MH, HM, and TK collected the samples. KW and HM conducted  
429 the laboratory analyses. KW and TK processed the data. KW and TK wrote the paper with substantial input from the other  
430 authors.

431 **Competing interests**

432 The authors declare that they have no conflict of interest.

433 **Acknowledgements.** This study was funded in part by Grants-in-Aid for Scientific Research (KAKENHI) grant numbers  
434 JP18H04156, 19K20500, and 19K12295 from the Japan Society for the Promotion of Science. We thank A. Kajita, K.  
435 Manabe, and S. Sueyoshi for help in field observations and N. Umegaki, H. Kimishima, and R. Makino for chemical  
436 analyses.

437 **References**

- 438 Abdullah, M.I. and Fredriksen, S.: Production, respiration and exudation of dissolved organic matter by the kelp *Laminaria*  
439 *hyperborea* along the west coast of Norway, J. Mar. Biol. Assoc. U. K., 84, 887–894,  
440 <https://doi.org/10.1017/S002531540401015Xh>, 2004.
- 441 Arrieta, J. M., Mayol, E., Hansman, R. L., Herndl, G. J., Dittmar, T., and Duarte, C. M.: Dilution limits dissolved organic  
442 carbon utilization in the deep ocean, *Science*, 348, 331–333, <https://doi.org/10.1126/science.1258955>, 2015.
- 443 Balotro, R. S., Isobe, A., Shimizu, M., Kaneda, A., Takeuchi, T., and Takeoka, H.: Circulation and Material Transport in  
444 Suo-Nada during Spring and Summer, *J. Oceanogr.*, 58, 759–773, <https://doi.org/10.1023/A:1022858710221>, 2002.
- 445 Barrón, C., Apostolaki, E. T., and Duarte, C. M.: Dissolved organic carbon fluxes by seagrass meadows and macroalgal beds,  
446 *Front. Mar. Sci.*, 1, 42, <https://doi.org/10.3389/fmars.2014.00042>, 2014.
- 447 Bauer, J. E. and Bianchi, T. S.: Dissolved Organic Carbon Cycling and Transformation, in: *Treatise on Estuarine and Coastal*  
448 *Science*, edited by: Wolanski, E. and McLusky, D. S., Academic Press, Sam Diego, CA, USA, 7–67,  
449 <https://doi.org/10.1016/B978-0-12-374711-2.00502-7>, 2011.
- 450 Bauer, J. E. and Druffel, E. R.: Ocean margins as a significant source of organic matter to the deep open ocean, *Nature*, 92,  
451 482–485, <https://doi.org/10.1038/33122>, 1998.
- 452 Bensoussan, N. and Gattuso, J.-P.: Community primary production and calcification in a NW Mediterranean ecosystem  
453 dominated by calcareous macroalgae, *Mar. Ecol. Progr. Ser.*, 334, 37–45, <https://doi.org/10.3354/meps334037>, 2007.
- 454 Chen, W. and Wangersky, P. J.: Rates of microbial degradation of dissolved organic carbon from phytoplankton cultures, *J.*  
455 *Plankton Res.*, 18, 1521–1533, [doi:10.1093/plankt/18.9.1521](https://doi.org/10.1093/plankt/18.9.1521), 1996.
- 456 Choi, H. G., Lee, K. H., Yoo, H. I., Kang, P. J., Kim, Y. S., and Nam, K. W.: Physiological differences in the growth of  
457 *Sargassum horneri* between the germling and adult stages, *J. Appl. Phycol.*, 20, 729–35, [https://doi.org/10.1007/s10811-](https://doi.org/10.1007/s10811-007-9281-5)  
458 007-9281-5, 2008.



459 Delille, B., Borges A. V., and Delille, D.: Influence of giant kelp beds (*Macrocystis pyrifera*) on diel cycles of pCO<sub>2</sub> and  
460 DIC in the Sub-Antarctic coastal area, *Estuar. Coast. Shelf Sci.*, 81, 114–122, <https://doi.org/10.1016/j.ecss.2008.10.004>,  
461 2009.

462 Delille, B., Dellile, D., Fiala, M., Prevost, C., and Frankignoulle. M.: Seasonal changes of pCO<sub>2</sub> over a subantarctic  
463 *Macrocystis* kelp bed, *Polar Biol.*, 23, 706–716, <https://doi.org/10.1007/s003000000142>, 2000.

464 Duarte, C. M.: Submerged aquatic vegetation in relation to different nutrient regimes, *Ophelia*, 41, 87–112,  
465 <https://doi.org/10.1080/00785236.1995.10422039>, 1995.

466 Duarte, C. M.: Reviews and syntheses: Hidden forests, the role of vegetated coastal habitats in the ocean carbon budget,  
467 *Biogeosciences*, 14, 301–310, <https://doi.org/10.5194/bg-14-301-2017>, 2017.

468 Duarte, C. M. and Krause-Jensen, D.: Export from Seagrass Meadows Contributes to Marine Carbon Sequestration, *Front.*  
469 *Mar. Sci.*, 4, 13, <https://doi.org/10.3389/fmars.2017.00013>, 2017.

470 Duarte, C. M. and Krause-Jensen, D.: Greenland Tidal Pools as Hot Spots for Ecosystem Metabolism and Calcification,  
471 *Estuar. Coast.*, 41, 1314–1321, doi:10.1007/s12237-018-0368-9, 2018.

472 Duarte, C. M., Losada, I. J., Hendriks, I. E., Mazarrasa, I., and Marbà, N.: The role of coastal plant communities for climate  
473 change mitigation and adaptation, *Nat. Clim. Change*, 3, 961–968, <https://doi.org/10.1038/nclimate1970>, 2013.

474 Falter, J. L., Atkinson, M. J., and Langdon, C.: Production–respiration relationships at different timescales within the  
475 Biosphere 2 coral reef biome, *Limnol. Oceanogr.*, 46, 1653–1660, <https://doi.org/10.4319/lo.2001.46.7.1653>, 2001.

476 Filbee-Dexter, K., Wernberg, T., Norderhaug, K. M., Ramirez-Llodra, E., and Pedersen, M. F.: Movement of pulsed  
477 resource subsidies from kelp forests to deep fjords, *Oecologia*, 187, 291–304, <https://doi.org/10.1007/s00442-018-4121-7>,  
478 2018.

479 Frankignoulle, M.: A complete set of buffer factors for acid/base CO<sub>2</sub> system in seawater, *J. Mar. Syst.*, 5, 111–118,  
480 [https://doi.org/10.1016/0924-7963\(94\)90026-4](https://doi.org/10.1016/0924-7963(94)90026-4), 1994.

481 Fulton, C. J., Abesamis, R. A., Berkström, C., Depczynski, M., Graham, N. A. J., Holmes, T. H., Kulbicki, M., Noble, M. M.,  
482 Radford, B. T., Tano, S., Tinkler, P., Wernberg, T., and Wilson, S. K.: Form and function of tropical macroalgal reefs in  
483 the Anthropocene, *Funct. Ecol.*, 33, 989–999, <https://doi.org/10.1111/1365-2435.13282>, 2019.

484 Gao, K. and Hua, W.: *In situ* growth rates of *Sargassum horneri* (Fucales, Phaeophyta), *Phycol. Res.*, 45, 55–57,  
485 <https://doi.org/10.1111/j.1440-1835.1997.tb00062.x>, 1997.

486 Hama, T., Yanagi, K., and Hama, J.: Decrease in molecular weight of photosynthetic products of marine phytoplankton  
487 during early diagenesis, *Limnol. Oceanogr.*, 49, 471–481, <https://doi.org/10.4319/lo.2004.49.2.0471>, 2004.

488 Hansell, D. A. and Carlson, C. A. (Eds.): *Biogeochemistry of Marine Dissolved Organic Matter*, Academic Press, San Diego,  
489 CA, USA, <https://doi.org/10.1016/C2012-0-02714-7>, 2015.

490 Ikawa, H. and Oechel, W. C.: Temporal variations in air-sea CO<sub>2</sub> exchange near large kelp beds near San Diego, California,  
491 *J. Geophys. Res. Oceans*, 120, 50–63, <https://doi.org/10.1002/2014JC010229>, 2015.

492 Jackson, G.A.: Modelling the growth and harvest yield of the giant kelp *Macrocystis pyrifera*, Mar. Biol., 95, 611–624,  
493 <https://doi.org/10.1007/BF00393105>, 1987.

494 Jackson, G.A. and Winant, C.D.: Effect of a kelp forest on coastal currents, Continent. Shelf Res., 2, 75–80,  
495 [https://doi.org/10.1016/0278-4343\(83\)90023-7](https://doi.org/10.1016/0278-4343(83)90023-7), 1983.

496 Jiang, Z., Fang, J., Mao, Y., Han, T., and Wang, G.: Influence of Seaweed Aquaculture on Marine Inorganic Carbon  
497 Dynamics and Sea-air CO<sub>2</sub> Flux, J. World Aquaculture Soc., 44, 133–140, <https://doi.org/10.1111/jwas.12000>, 2013.

498 Kamiya, M., Nishio, T., Yokoyama, A., Yatsuya, K., Nishigaki, T., Yoshikawa, S., and Ohki, K.: Seasonal variation of  
499 phlorotannin in sargassacean species from the coast of the Sea of Japan, Phycol. Res., 58, 53–61,  
500 <https://doi.org/10.1111/j.1440-1835.2009.00558.x>, 2010.

501 Kirchman, D. L., Suzuki, Y., Garside, C., and Ducklow, H. W.: High turnover rates of dissolved organic carbon during a  
502 spring phytoplankton bloom, Nature, 352, 612–614, <https://doi.org/10.1038/352612a0>, 1991.

503 Kokubu, Y., Rothäusler, E., Filippi, J.-B., Durieux, E. D. H., and Komatsu, T.: Revealing the deposition of macrophytes  
504 transported offshore: Evidence of their long-distance dispersal and seasonal aggregation to the deep sea, Sci. Rep., 9, 4331,  
505 <https://doi.org/10.1038/s41598-019-39982-w>, 2019.

506 Kondo, J.: Atmosphere Science near the Ground Surface, University of Tokyo Press, Tokyo, Japan, 2000.

507 Kowalik, D. A., Nickols, K. J., Leary, P. R., Litvin, S. Y., Bell, T. W., Luthin, T., Lummis, S., Mucciarone, D. A., and  
508 Dunbar, R. B.: A year in the life of a central California kelp forest: physical and biological insights into biogeochemical  
509 variability, Biogeosciences, 14, 31–44, <https://doi.org/10.5194/bg-14-31-2017>, 2017.

510 Krause-Jensen, D. and Duarte, C. M.: Substantial role of macroalgae in marine carbon sequestration, Nat. Geosci., 9, 737–  
511 742, <https://doi.org/10.1038/ngeo2790>, 2016.

512 Krause-Jensen, D., Duarte, C. M., Hendriks, I. E., Meire, L., Blicher, M. E., Marbà, N., and Sejr, M. K.: Macroalgae  
513 contribute to nested mosaics of pH variability in a subarctic fjord, Biogeosciences, 12, 4895–4911,  
514 <http://doi.org/10.5194/bg-12-4895-2015>, 2015.

515 Krause-Jensen, D., Lavery, P., Serrano, O., Marbà, N., Masque, P., and Duarte, C. M.: Sequestration of macroalgal carbon:  
516 the elephant in the Blue Carbon room, Biol. Lett., 14, 20180236, <http://doi.org/10.1098/rsbl.2018.0236>, 2018.

517 Krause-Jensen, D., Marbà, N., Sanz-Martin, M., Hendriks, I. E., Thyrring, J., Carstensen, J., Sejr, M. K., Duarte, C. M.:  
518 Long photoperiods sustain high pH in Arctic kelp forests, Sci. Adv., 2, e1501938, <https://doi.org/10.1126/sciadv.1501938>,  
519 2016.

520 Kubo, A., Yamamoto-Kawai, M., and Kanda, J.: Seasonal variations in concentration and lability of dissolved organic carbon  
521 in Tokyo Bay, Biogeosciences, 12, 239–279, <https://doi.org/10.5194/bg-12-269-2015>, 2015.

522 Kuwae, T., Kanda, J., Kubo, A., Nakajima, F., Ogawa, H., Sohma, A., and Suzumura, M.: CO<sub>2</sub> Uptake in the Shallow  
523 Coastal Ecosystems Affected by Anthropogenic Impacts, in: Blue Carbon in Shallow Coastal Ecosystems: Carbon  
524 Dynamics, Policy, and Implementation, edited by: Kuwae, T. and Hori, M., Springer, Singapore, 295–319,  
525 [https://doi.org/10.1007/978-981-13-1295-3\\_11](https://doi.org/10.1007/978-981-13-1295-3_11), 2019.

526 Lønborg, C. and Álvarez-Salgado, X. A.: Recycling versus export of bioavailable dissolved organic matter in the coastal  
527 ocean and efficiency of the continental shelf pump, *Global Biogeochem. Cy.*, 26, GB3018,  
528 <https://doi.org/10.1029/2012GB004353>, 2012.

529 Macreadie, P. I., Anton, A., Raven, J. A., Beaumont, N., Connolly, R. M., Friess, D. A., Kelleway, J. J., Kennedy, H.,  
530 Kuwae, T., Lavery, P. S., Lovelock, C. E., Smale, D. A., Apostolaki, E. T., Atwood, T. B., Baldock, J., Bianchi, T. S.,  
531 Chmura, G. L., Eyre, B. D., Fourqurean, J. W., Hall-Spencer, J. M., Huxham, M., Hendriks, I. E., Krause-Jensen, D.,  
532 Laffoley, D., Luisetti, T., Marbà, N., Masque, P., McGlathery, K. J., Megonigal, J. P., Murdiyarso, D., Russell, B. D.,  
533 Santos, R., Serrano, O., Silliman, B. R., Watanabe, K., and Duarte, C. M.: The future of Blue Carbon science, *Nat. Comm.*,  
534 10, 3998, <https://doi.org/10.1038/s41467-019-11693-w>, 2019.

535 Maher, D. T. and Eyre, B. D.: Benthic fluxes of dissolved organic carbon in three temperate Australian estuaries:  
536 Implications for global estimates of benthic DOC fluxes, *J. Geophys. Res. Biogeosciences*, 115, G04039,  
537 <https://doi.org/10.1029/2010JG001433>, 2010.

538 Martin, S., Clavier, J., Chauvaud, L., and Thouzeau, G.: Community metabolism in temperate maerl beds. I. Carbon and  
539 carbonate fluxes, *Mar. Ecol. Prog. Ser.*, 335, 19-29, <https://doi.org/10.3354/meps335019>, 2007.

540 McGillis, W. R., Edson, J. B., Ware, J. D., Dacey, J. W. H., Hare, J. E., Fairall, C. W., and Wanninkhof, R.: Carbon dioxide  
541 flux techniques performed during GasEx-98., *Mar. Chem.*, 75, 267–280, [https://doi.org/10.1016/S0304-4203\(01\)00042-1](https://doi.org/10.1016/S0304-4203(01)00042-1),  
542 2001.

543 Mcleod, E., Chmura, G. L., Bouillon, S., Salm, R., Björk, M., Duarte, C. M., Lovelock, C. E., Schlesinger, W. H., and  
544 Silliman, B. R.: A blueprint for blue carbon: toward an improved understanding of the role of vegetated coastal habitats in  
545 sequestering CO<sub>2</sub>, *Front. Ecol. Environ.*, 9, 552–560, <https://doi.org/10.1890/110004>, 2011.

546 Middelboe, A. L. and Hansen, P. J.: High pH in shallow-water macroalgal habitats, *Mar. Ecol. Progr. Ser.*, 338, 107–117,  
547 <https://doi.org/10.3354/meps338107>, 2007.

548 Miyajima T. and Hamaguchi M.: Carbon Sequestration in Sediment as an Ecosystem Function of Seagrass Meadows, in:  
549 Blue Carbon in Shallow Coastal Ecosystems: Carbon Dynamics, Policy, and Implementation, edited by: Kuwae, T. and  
550 Hori, M., Springer, Singapore, 33–71, [https://doi.org/10.1007/978-981-13-1295-3\\_2](https://doi.org/10.1007/978-981-13-1295-3_2), 2019.

551 Nellemann, C., Corcoran, E., Duarte, C. M., Valdés, L., De Young, C., Fonseca, L., and Grimsditch, G.: Blue carbon. A  
552 rapid response assessment, United Nations Environmental Programme, Arendal, Norway, 2009.

553 Ogawa, H., Amagai, Y., Koike, I., Kaiser, K., and Benner, R.: Production of Refractory Dissolved Organic Matter by  
554 Bacteria, *Science*, 292, 917–920, <https://doi.org/10.1126/science.1057627>, 2001.

555 Ogawa, H., Fukuda, R., and Koike, I.: Vertical distributions of dissolved organic carbon and nitrogen in the Southern Ocean,  
556 *Deep Sea Res. I*, 46, 1809–1826, [https://doi.org/10.1016/S0967-0637\(99\)00027-8](https://doi.org/10.1016/S0967-0637(99)00027-8), 1999.

557 Pedersen, M. F., Filbee-Dexter, K., Norderhaug, K. M., Fredriksen, S., Frisk, N. L., Fagerli, C. W., and Wernberg, T.:  
558 Detrital carbon production and export in high latitude kelp forests, *Oecologia*, [https://doi.org/10.1007/s00442-019-04573-](https://doi.org/10.1007/s00442-019-04573-z)  
559 [z](https://doi.org/10.1007/s00442-019-04573-z), 2019.

560 Pedersen, M. F., Stæhr, P. A., Wernberg, T., and Thomsen, M. S.: Biomass dynamics of exotic *Sargassum muticum* and  
561 native *Halidrys siliquosa* in Limfjorden, Denmark—Implications of species replacements on turnover rates, *Aquat. Bot.*,  
562 83, 31–47, <https://doi.org/10.1016/j.aquabot.2005.05.004>, 2005.

563 Pessarrodona, A., Moore, P. J., Sayer, M. D. J., and Smale, D. A.: Carbon assimilation and transfer through kelp forests in  
564 the NE Atlantic is diminished under a warmer ocean climate, *Global Change Biol.*, 24, 4386–4398,  
565 <https://doi.org/10.1111/gcb.14303>, 2018.

566 Pfister, C. A., Altabet, M. A., and Weigel, B. L.: Kelp beds and their local effects on seawater chemistry, productivity, and  
567 microbial communities, *Ecology*, 100, e02798, <https://doi.org/10.1002/ecy.2798>, 2019.

568 Powers, L. C., Hertkorn, N., McDonald, N., Schmitt-Kopplin, P., Del Vecchio, R., Blough, N. V., and Gonsior, M.:  
569 *Sargassum* sp. act as a Large Regional Source of Marine Dissolved Organic Carbon and Polyphenols, *Global Biogeochem.*  
570 *Cy.*, <https://doi.org/10.1029/2019GB006225>, 2019.

571 Queirós, A. M., Stephens, N., Widdicombe, S., Tait, K., McCoy, S. J., Ingels, J., Rühl, S., Airs, R., Beesley, A., Carnovale,  
572 G., Cazenave, P., Dashfield, S., Hua, E., Jones, M., Lindeque, P., McNeill, C. L., Nunes, J., Parry, H., Pascoe, C.,  
573 Widdicombe, C., Smyth, T., Atkinson, A., Krause-Jensen, D., and Somerfield, P. J.: Connected macroalgal-sediment  
574 systems: blue carbon and food webs in the deep coastal ocean, *Ecol. Monogr.*, 89, e01366,  
575 <https://doi.org/10.1002/ecm.1366>, 2019.

576 Randall, J., Wotherspoon, S., Ross, J., Hermand, J. P., and Johnson, C. R.: An *in situ* study of production from diel oxygen  
577 modelling, oxygen exchange, and electron transport rate in the kelp *Ecklonia radiata*, *Mar. Ecol. Prog. Ser.*, 615, 51–65,  
578 <https://doi.org/10.3354/meps12919>, 2019.

579 Raven, J.: Blue carbon: past, present and future, with emphasis on macroalgae, *Biol. Lett.*, 14, 20180336,  
580 <http://doi.org/10.1098/rsbl.2018.03363>, 2018.

581 R Core Team: R: A language and environment for statistical computing, R Foundation for Statistical Computing, Vienna,  
582 Austria, <https://www.R-project.org/>, 2019.

583 Reed, D. C., Carlson, C. A., Halewood, E. R., Nelson, J. C., Harrer, S. L., Rassweiler, A., and Miller, R. J.: Patterns and  
584 controls of reef-scale production of dissolved organic carbon by giant kelp *Macrocystis pyrifera*, *Limnol. Oceanogr.*, 60,  
585 1996–2008, <https://doi.org/10.1002/lno.10154>, 2015.

586 Rosman, J. H., Koseff, J. R., Monismith, S. G., and Grover, J.: A field investigation into the effects of a kelp forest  
587 (*Macrocystis pyrifera*) on coastal hydrodynamics and transport, *J. Geophys. Res. Oceans*, 112, 1–16,  
588 <https://doi.org/10.1029/2005JC003430>, 2007.

589 Smith, S. V.: Marine macrophytes as a global carbon sink, *Science*, 211, 838–840,  
590 <https://doi.org/10.1126/science.211.4484.838>, 1981.

591 Steinberg, P. D.: Biogeographical variation in brown algal polyphenolics and other secondary metabolites: comparison  
592 between temperate Australasia and North America, *Oecologia*, 78, 373–82, <https://doi.org/10.1007/BF00379112>, 1989.

593 Swanson, A. K. and Druehl, L. D.: Induction, exudation and the UV protective role of kelp phlorotannins, *Aquat. Bot.*, 73,  
594 241–253, [https://doi.org/10.1016/S0304-3770\(02\)00035-9](https://doi.org/10.1016/S0304-3770(02)00035-9), 2002.

595 Tokoro, T., Hosokawa, S., Miyoshi, E., Tada, K., Watanabe, K., Montani, S., Kayanne, H., and Kuwae, T.: Net uptake of  
596 atmospheric CO<sub>2</sub> by coastal submerged aquatic vegetation, *Global Change Biol.*, 20, 1873–1884,  
597 <https://doi.org/10.1111/gcb.12543>, 2014.

598 Tokoro, T., Watanabe, K., Tada, K., and Kuwae, T.: Air–Water CO<sub>2</sub> Flux in Shallow Coastal Waters: Theory, Methods, and  
599 Empirical Studies, in: *Blue Carbon in Shallow Coastal Ecosystems: Carbon Dynamics, Policy, and Implementation*, edited  
600 by: Kuwae, T. and Hori, M., Springer, Singapore, 153–184, [https://doi.org/10.1007/978-981-13-1295-3\\_6](https://doi.org/10.1007/978-981-13-1295-3_6), 2019.

601 Towle, D. W. and Pearse, J. S.: Production of the giant kelp, *Macrocystis*, by in situ incorporation of <sup>14</sup>C in polyethylene  
602 bags, *Limnol. Oceanogr.*, 18, 155–159, <https://doi.org/10.4319/lo.1973.18.1.0155>, 1973.

603 **Trevathan-Tackett, S. M., Jeffries, T. C., Macreadie, P. I., Manojlovic, B., and Ralph, P.: Long-term decomposition captures**  
604 **key steps in microbial breakdown of seagrass litter, *Sci. Total Environ.*, 705, 135806,**  
605 **<https://doi.org/10.1016/j.scitotenv.2019.135806>, 2020.**

606 Trevathan-Tackett, S. M., Kelleway, J., Macreadie, P. I., Beardall, J., Ralph, P., and Bellgrove, A.: Comparison of marine  
607 macrophytes for their contributions to blue carbon sequestration, *Ecology*, 96, 3043–3057, <https://doi.org/10.1890/15-0149.1>, 2015.

609 Wada, S., Aoki, M. N., Mikami, A., Komatsu, T., Tsuchiya, Y., Sato, T., Shinagawa, H., and Hama, T.: Bioavailability of  
610 macroalgal dissolved organic matter in seawater, *Mar. Ecol. Prog. Ser.*, 370, 33–44, <https://doi.org/10.3354/meps07645>,  
611 2008.

612 Wada, S., Aoki, M. N., Tsuchiya, Y., Sato, T., Shinagawa, H., and Hama, T.: Quantitative and qualitative analyses of  
613 dissolved organic matter released from *Ecklonia cava* Kjellman, in Oura Bay, Shimoda, Izu Peninsula, Japan, *J. Exp. Mar.*  
614 *Biol. Ecol.*, 349, 344–358, <https://doi.org/10.1016/j.jembe.2007.05.024>, 2007.

615 Wada, S. and Hama, T.: The contribution of macroalgae to the coastal dissolved organic matter pool, *Estuar. Coast. Shelf*  
616 *Sci.*, 129, 77–85, <https://doi.org/10.1016/j.ecss.2013.06.007>, 2013.

617 **Wahl, M., Schneider Covachá, S., Saderne, V., Hiebenthal, C., Müller, J. D., Pansch, C., and Sawall, Y.: Macroalgae may**  
618 **mitigate ocean acidification effects on mussel calcification by increasing pH and its fluctuations, *Limnol. Oceanogr.*, 63,**  
619 **<https://doi.org/10.1002/lno.10608>, 2018.**

620 Wanninkhof, R.: Relationship between wind-speed and gas-exchange over the ocean, *J. Geophys. Res. Oceans*, 97, 7373–  
621 7382, <https://doi.org/10.1029/92JC00188>, 1992.

622 Watanabe, K. and Kuwae, T.: How organic carbon derived from multiple sources contributes to carbon sequestration  
623 processes in a shallow coastal system?, *Global Change Biol.*, 21, 2612–2623, <https://doi.org/10.1111/gcb.12924>, 2015.

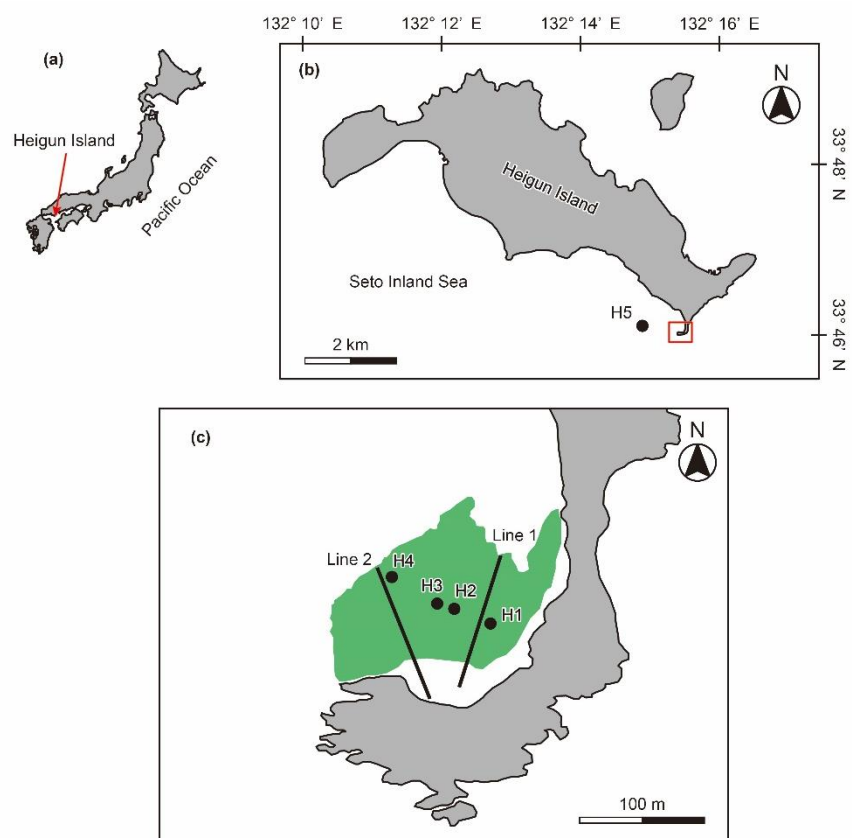
624 Weiss, R. F.: Carbon dioxide in water and seawater: the solubility of a non-ideal gas, *Mar. Chem.*, 2, 203–215,  
625 [https://doi.org/10.1016/0304-4203\(74\)90015-2](https://doi.org/10.1016/0304-4203(74)90015-2), 1974.

626 Yoshida, G., Hori, M., Shimabukuro, H., Hamaoka, H., Onitsuka, T., Hasegawa, N., Muraoka, D., Yatsuya, K., Watanabe,  
627 K., and Nakaoka, M.: Carbon Sequestration by Seagrass and Macroalgae in Japan: Estimates and Future Needs, in: Blue  
628 Carbon in Shallow Coastal Ecosystems: Carbon Dynamics, Policy, and Implementation, edited by: Kuwae, T. and Hori,  
629 M., Springer, Singapore, 101–127, [https://doi.org/10.1007/978-981-13-1295-3\\_4](https://doi.org/10.1007/978-981-13-1295-3_4), 2019.

630 Yoshida, G., Yoshikawa, K., and Terawaki, T.: Growth and maturation of two populations of *Sargassum horneri* (Fucales,  
631 Phaeophyta) in Hiroshima Bay, the Seto Inland Sea, Fish. Sci., 67, 1023–1029, <https://doi.org/10.1046/j.1444->  
632 2906.2001.00357.x, 2001.

633 Zeebe, R. E. and Wolf-Gladrow, D.: CO<sub>2</sub> in Seawater: Equilibrium, Kinetics, Isotopes, Elsevier, Amsterdam, Netherlands,  
634 2001.

635

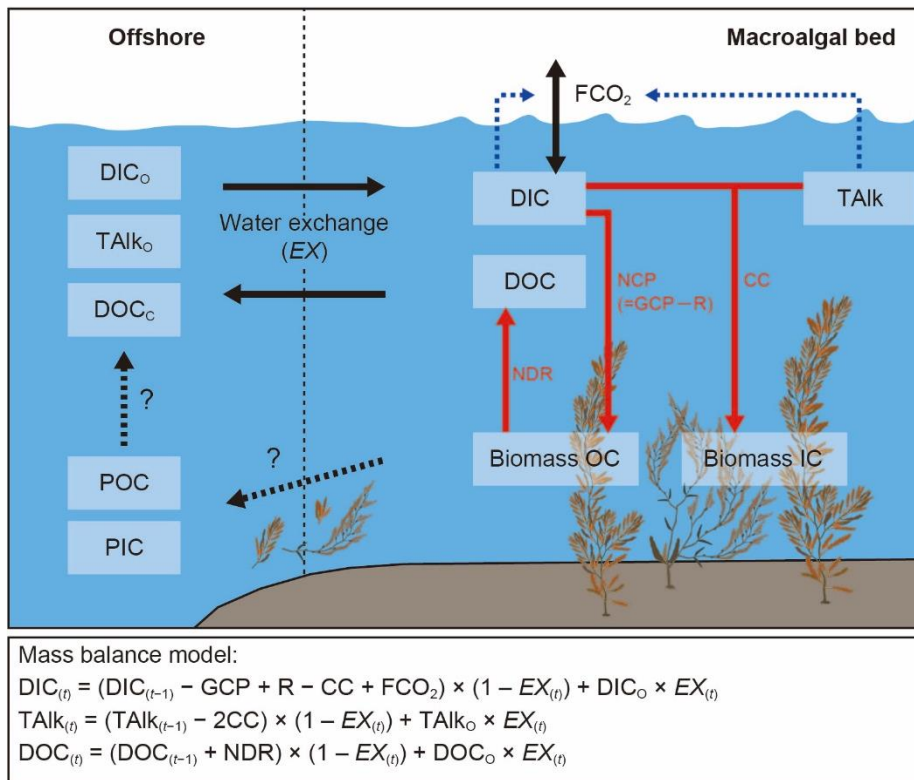


637

638 **Figure 1:** Maps of Heigun Island and the locations of sampling stations (H1–H5) and transect lines. Green shading indicates  
639 the area occupied by the macroalgal bed.

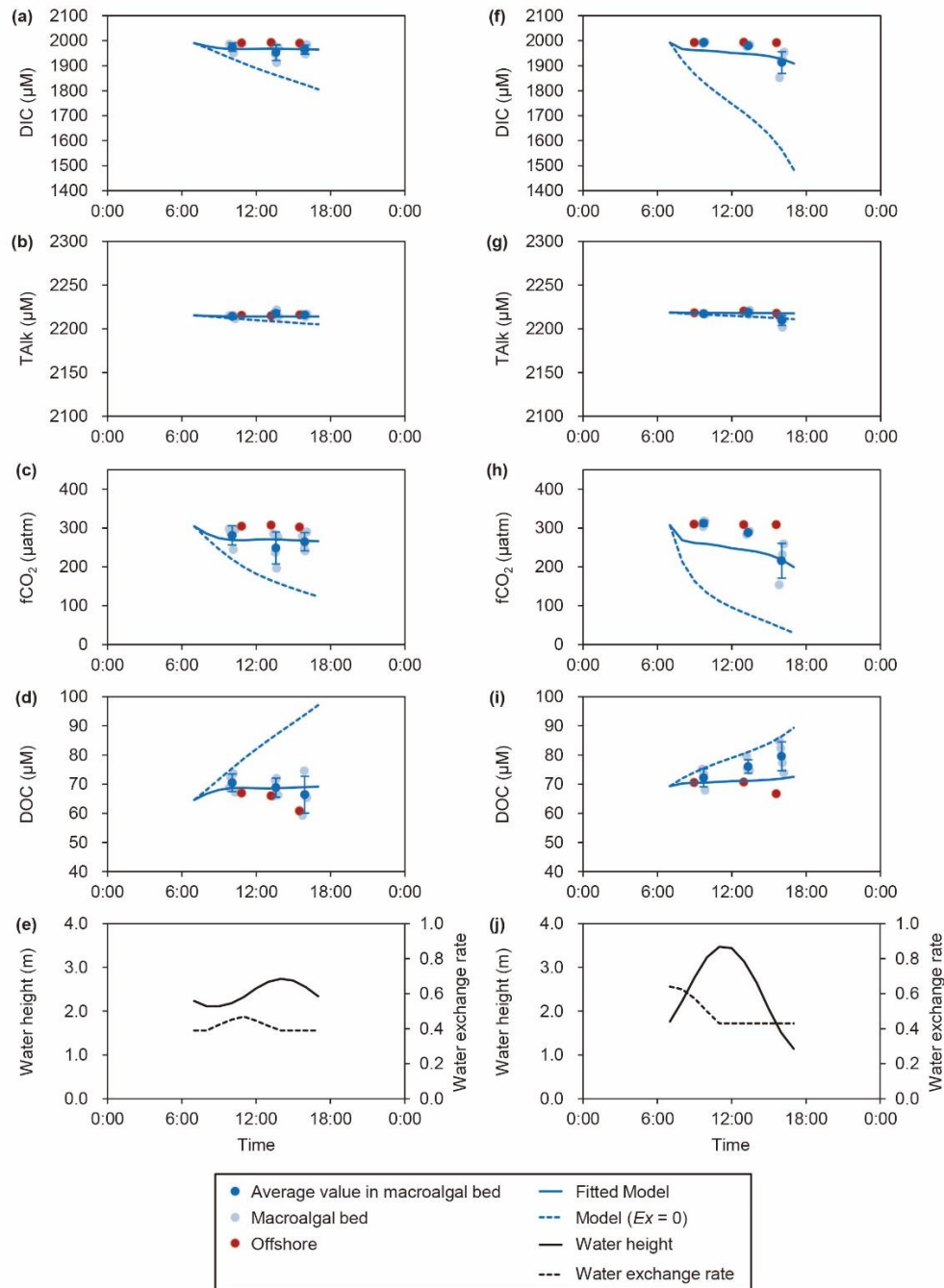
640





641  
642  
643  
644  
645  
646  
647  
648  
649  
650  
651  
652  
653  
654  
655

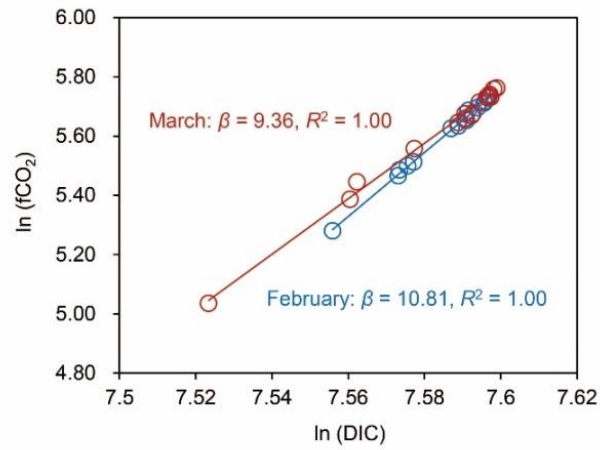
**Figure 2:** Schematic diagram of the different carbon pools and flows in and around macroalgal beds. Black arrows indicate carbon flows between macroalgal beds and the outside of the system; black dashed arrows with question marks denote carbon flows that were not evaluated in this study; red arrows indicate effects of community metabolism on carbon pools in macroalgal beds. Blue dashed arrows indicate that dissolved inorganic carbon (DIC) and total alkalinity (TALK) regulate air-water CO<sub>2</sub> exchange fluxes (FCO<sub>2</sub>). DIC concentrations in macroalgal beds are regulated by net community production (NCP), community calcification (CC), FCO<sub>2</sub>, and mixing with offshore DIC (DIC<sub>O</sub>). NCP is the difference between gross community production (GCP) and community respiration (R). TALK in macroalgal beds is regulated by CC and mixing with offshore TALK (TALK<sub>O</sub>). Dissolved organic carbon (DOC) concentrations in macroalgal beds are regulated by net DOC release (NDR) and mixing with offshore DOC (DOC<sub>O</sub>). Organic carbon (OC) and inorganic carbon (IC) of macroalgal biomass are produced by NCP and CC, respectively, and some of each is exported to the offshore in particulate form (POC and PIC, respectively). Mass balance models simulated the diurnal changes and budgets of DIC, TALK, and DOC in the macroalgal bed at hourly time steps (*t*) in this study.



657

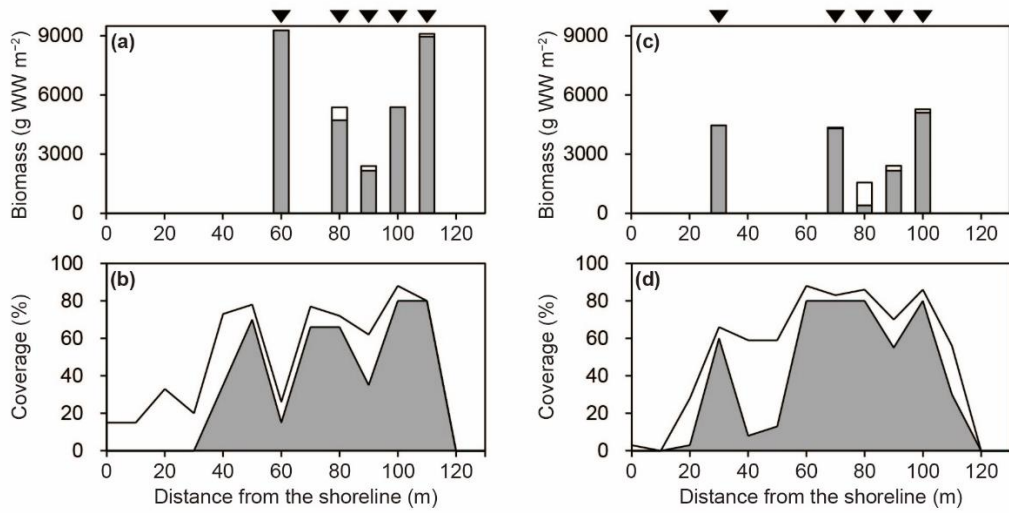
658 **Figure 3:** Temporal changes in dissolved inorganic carbon (DIC), total alkalinity (TAlk), fugacity of  $\text{CO}_2$  ( $f\text{CO}_2$ ), dissolved  
 659 organic carbon (DOC), water height, and water exchange rate ( $EX$ ) in February (a–e) and March (f–j). Modelled values of  
 660 chemical parameters were estimated by using mass balance models. Error bars show standard deviations. Blue dashed lines  
 661 show the model results if the  $EX$  is zero. Details regarding observed values are provided in Table S2 in the Supplement.

662  
663



664  
665 **Figure 4:** Plots of fugacity of CO<sub>2</sub> (fCO<sub>2</sub>) versus dissolved inorganic carbon (DIC) and regression lines used to determine  
666 the homogeneous buffer factors ( $\beta$ ) as slopes.

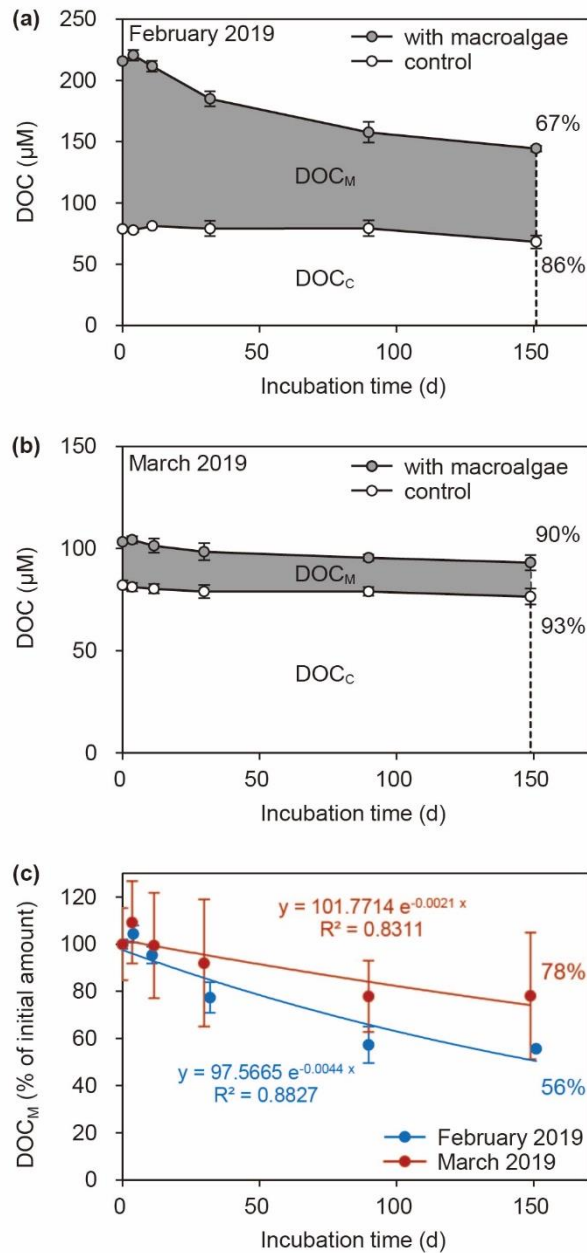
667



669

670 **Figure 5:** Biomass and coverage of macroalgae along transect line 1 (a, b) and line 2 (c, d) in March 2019. Grey and white  
 671 shading indicate *Sargassum* algae and other macroalgae, respectively. Black arrows indicate sampling locations for  
 672 macroalgal biomass.

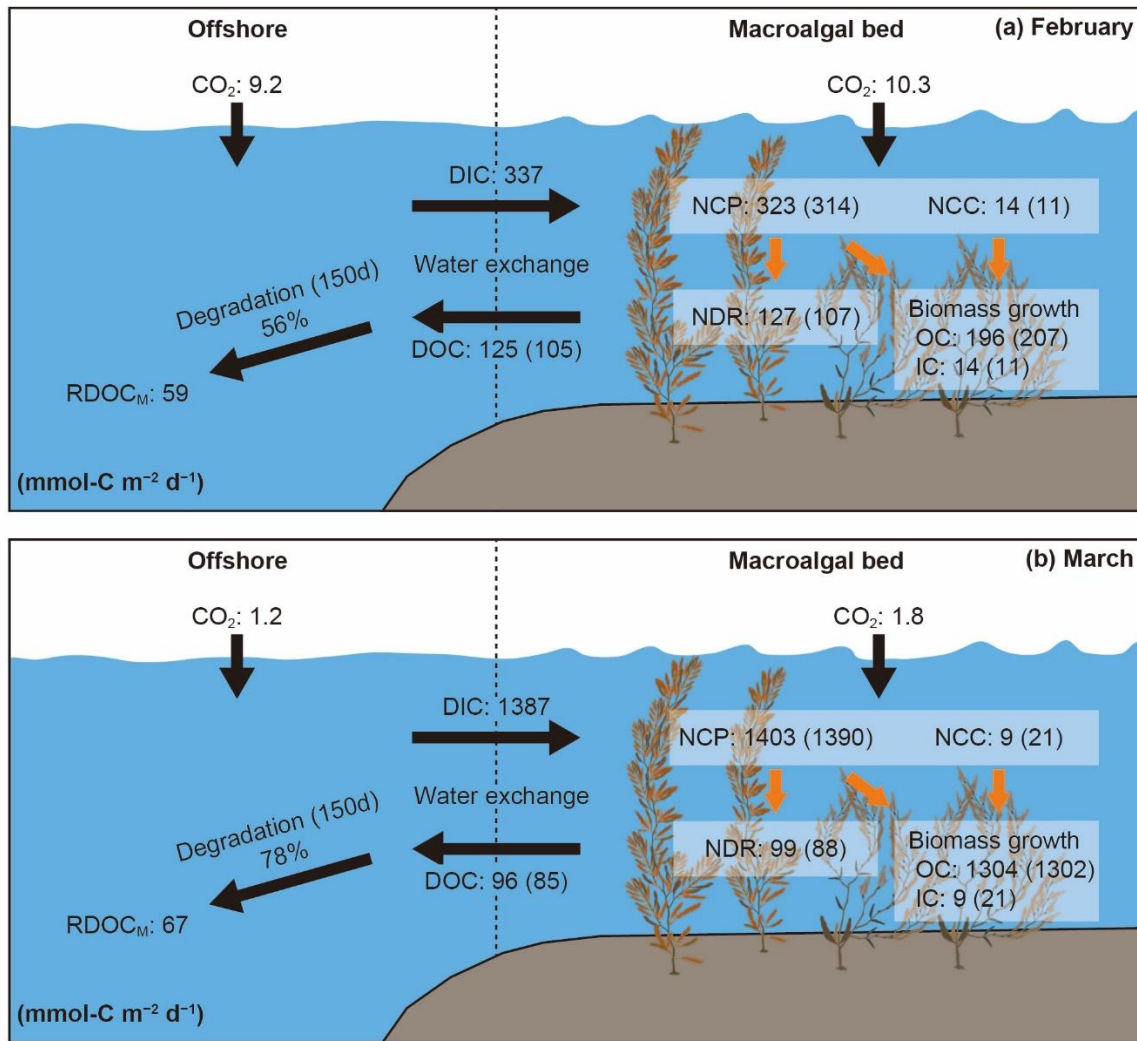
673



675

676 **Figure 6:** Time course of dissolved organic carbon (DOC) concentrations during the degradation experiments in (a)  
 677 February and (b) March and (c) percentage of DOC derived from macroalgae during both experiments. Shading indicates the  
 678 concentration of DOC derived from macroalgae (DOC<sub>M</sub>), which was equated to the difference between the DOC  
 679 concentration in the macroalgae bag and the DOC concentration in the control bag (DOC<sub>C</sub>). Percentages in panels (a) and  
 680 (b) are averaged final percentage of DOC<sub>M</sub> and DOC<sub>C</sub> remaining in each treatment after 150 days.

681



683

684 **Figure 7:** Carbon flows and community metabolism (NCP, net community production; NCC, net community calcification;  
 685 NDR, net DOC release) in the macroalgal bed. NCP, NCC, and NDR were calculated using the results of field bag  
 686 experiments (details are available in Table S1 in the Supplement). Biomass growth in terms of organic carbon (OC) was  
 687 calculated by subtracting NDR from NCP. Biomass growth in terms of inorganic carbon (IC) was the same as NCC. DIC and  
 688 DOC flows via water exchange were estimated by mass balance modelling (details are available in Table 3). Community  
 689 metabolism, biomass growth, and DOC outflow indicate the sum of macroalgal and planktonic carbon flows. The carbon  
 690 flows due solely to macroalgae are shown in parentheses. Carbon fluxes were calculated in units of millimoles per square  
 691 metre of the surface area of the macroalgal bed per day. RDOC<sub>M</sub> indicates refractory DOC released by macroalgae.

692

693

694 **Table 1:** Carbon metabolism, surface water temperature, photosynthetic photon flux, length of photoperiod, and chlorophyll  
 695 fluorescence in February and March 2019. For macroalgae, mean  $\pm$  standard deviation are shown. Average water depth and  
 696 biomass in the bed were used for calculating metabolic rates.

697

Variables	Units	February 2019	March 2019
Macroalgae			
Net community production	mmol-C m <sup>-2</sup> d <sup>-1</sup>	314 $\pm$ 131	1390 $\pm$ 643
Gross community production	mmol-C m <sup>-2</sup> d <sup>-1</sup>	583 $\pm$ 130	1657 $\pm$ 632
Community respiration	mmol-C m <sup>-2</sup> d <sup>-1</sup>	269 $\pm$ 12	267 $\pm$ 114
Net DOC release	mmol-C m <sup>-2</sup> d <sup>-1</sup>	107 $\pm$ 36	88 $\pm$ 37
Net community calcification	mmol-C m <sup>-2</sup> d <sup>-1</sup>	11 $\pm$ 7	21 $\pm$ 23
Control (phytoplankton)			
Net community production	mmol-C m <sup>-2</sup> d <sup>-1</sup>	9	13
Gross community production	mmol-C m <sup>-2</sup> d <sup>-1</sup>	23	23
Community respiration	mmol-C m <sup>-2</sup> d <sup>-1</sup>	14	10
Net DOC release	mmol-C m <sup>-2</sup> d <sup>-1</sup>	20	11
Net community calcification	mmol-C m <sup>-2</sup> d <sup>-1</sup>	3	-12
Surface water temperature	°C	12.0 $\pm$ 0.2	12.4 $\pm$ 0.1
Photosynthetic photon flux	$\mu$ mol m <sup>-2</sup> s <sup>-1</sup>	674 $\pm$ 595	1311 $\pm$ 202
Length of photoperiod	h	11	12.5
Chlorophyll <i>a</i> concentration	$\mu$ g L <sup>-1</sup>	0.3	0.8

698

699



700

701 **Table 2:** Root mean square errors (RMSEs) for best-fitting models and models assuming that water exchange rate (*EX*) was  
702 zero. RMSEs were calculated for the *z*-scores of DIC, TAlk, DOC, and fCO<sub>2</sub> values, which were differences from the mean  
703 observed values divided by the standard deviations. The best-fitting model that minimized the averaged RMSEs for these  
704 four parameters was determined for each survey.

705

Variables	February 2019		March 2019	
	Best-fitting model	Model w/o <i>EX</i>	Best-fitting model	Model w/o <i>EX</i>
DIC	0.39	4.44	0.68	6.74
TAlk	0.99	3.52	0.97	0.62
DOC	0.41	4.46	1.08	1.04
fCO <sub>2</sub>	0.40	2.99	0.72	4.13
Mean	0.55	3.85	0.86	3.13

706

707

708

709 **Table 3:** Water exchange rates ( $EX_r$  and  $EX_{tide}$ ),  $FCO_2$ , DIC exchange, and DOC exchange, which were estimated by using  
710 mass balance models. Carbon fluxes were calculated as millimoles per square metre of the surface area of the algal bed per  
711 day.

712

Variables	Units	February 2019	March 2019
$EX_r$	% h <sup>-1</sup>	39	43
$EX_{tide}$	% h <sup>-1</sup>	0–13	0–26
$FCO_2$ in macroalgal bed	mmol-C m <sup>-2</sup> d <sup>-1</sup>	10.3	1.8
$FCO_2$ in offshore	mmol-C m <sup>-2</sup> d <sup>-1</sup>	9.2	1.2
DIC exchange	mmol-C m <sup>-2</sup> d <sup>-1</sup>	337	1387
DOC exchange	mmol-C m <sup>-2</sup> d <sup>-1</sup>	-125	-96

713

714